NASA CONTRACTOR REPORT

NASA CR-979

NASA CR-979

MICROWAVE TECHNIQUE DEVELOPMENT FOR ADVANCED RADIO ASTRONOMY AND RADIOMETRY MISSIONS

by B. M. Schiffman and Leo Young

Prepared by
STANFORD RESEARCH INSTTITUTE
Menlo Park, Calif.
for Electronics Research Center

NATIONAL AERONAUTICS AND SPACE ADMINISTRATION • WASHINGTON, D. C. • JANUARY 1968

NASA CR-979

MICROWAVE TECHNIQUE DEVELOPMENT FOR ADVANCED RADIO ASTRONOMY AND RADIOMETRY MISSIONS

By B. M. Schiffman and Leo Young

Prepared under Contract No. NAS 12-126 by
STANFORD RESEARCH INSTITUTE
Menlo Park, Calif.

for Electronics Research Center

NATIONAL AERONAUTICS AND SPACE ADMINISTRATION

For sale by the Clearinghouse for Federal Scientific and Technical Information
Springfield, Virginia 22151 – CFSTI price $3.00

ABSTRACT

A scale model ($f_o \approx 20\,GHz$) of a Solc-type birefringent wave filter for millimeter wavelengths is described. The filter consists of five cascaded identical half-wave plates, or crystals, each composed of an artificial anisotropic dielectric medium with its reference axis tilted at some prescribed angle to the plane of the input polarization. The design and analysis of an individual plate, using R. E. Collin's second-order theory of the birefringence of artificial anisotropic dielectrics, and the analysis of multielement filters (filters composed of many plates), aided by J. W. Evans's matrix method, are discussed. The experimental filter was tested in the range of 18-33 GHz, and its measured performance was found to compare well with the theoretical performance over a major portion of the range of frequencies used in the tests.

A synthesis procedure for optimum (equal-ripple stop band) response multielement filters is given, together with tables of plate angles for such filters. This procedure combines the Fourier approximation method of C. L. Dolph with the general synthesis method of S. E. Harris.

CONTENTS

CONTENTS (Concluded)

ILLUSTRATIONS

ILLUSTRATIONS (Concluded)

TABLES

PURPOSE

The purpose of this contract is to explore the possibility of utilizing optical birefringent filter techniques at millimeter wavelengths. The major goal of this effort is the construction and test of a multielement birefringent scale-model filter to operate at microwave frequencies.

I INTRODUCTION

A. GENERAL

The expansion of radio communication into the millimeter region depends either on the development of new techniques or the adaptation of existing techniques in new fields. The research reported herein falls in the latter category: an optical birefringent filter serves as the prototype for a millimeter-wave filter. As with almost all research, there is cross-fertilization; the optimum birefringent filter synthesis technique developed here is useful for optical filters as well as millimeter-wave filters.

The scope of this research includes the following: the design and testing of a scale model of a plate of artificial birefringent medium for the millimeter-wave region; the construction and testing of an experimental filter composed of several plates; and the investigation of methods of synthesizing optimum configurations of the plates of a filter, with a view toward providing convenient tables of filter designs (plate angles).

Although radio-frequency and optical waves are qualitatively the same, they require different techniques, which are generally not interchangeable. However, optical technology is more easily adapted to lower frequencies than the other way round. It is quite natural, therefore, to consider the use of optical filter techniques that were originally developed to exploit the birefringence property of certain naturally occurring transparent crystals, such as quartz and calcite, for millimeter or shorter wavelengths. This idea was first proposed by one of the authors (LY).[1]* The motivation, of course, is that microwave filter techniques are unsatisfactory at millimeter wavelengths. Conventional waveguide filters ordinarily require components comparable in size to a half-wavelength. Not

---

* References are given at the end of the report.

only are such items difficult and costly to construct for the millimeter wave region, but transmission loss rises rapidly and power-handling capacity decreases as frequency goes up. Furthermore, coherent power sources have an upper limit on power that decreases as frequency increases, so that the combination of high transmission loss and low available power can easily become intolerable.

Birefringent filters are generally used with waves propagating as a "parallel beam" in free space, rather than with guided waves. Power density is then much less than in waveguides of small cross section, and dispersion as in hollow waveguides is no longer a problem. Metal losses are eliminated, to be replaced by relatively mild dielectric losses. Birefringent filters were first invented in 1933 by Lyot,[2] a French astronomer. These first filters required crystals or plates of unequal length and lossy polarizers between each pair of adjacent plates. Later, Solc,[3-6] in Czechoslovakia, invented the form of filter in which all plates are of equal length and only two polarizers, one at each terminal, are required. The Solc-type filter is the subject of this research.

Cascades of birefringent crystals have been used in optics not only as filters but as demodulators of light[7] and as broadband quarter-wave plates.[8] The analytical techniques in all these applications are similar, as are the construction techniques. This report is concerned only with filters, particularly those designed to have small and equal ripples in the pass band. (Previous birefringent-filter designs have suffered from large reflection ripples at the edges of the pass band.)

Optical birefringent filters have the advantage of very narrow pass bands,[9] owing to the large number of optical wavelengths in the path through the birefringent material. In this respect they are much superior to optical interference filters. The presentation of an exact design theory, plus numerical tables, should therefore be of some significance. The experimental confirmation of theories relating to the design of birefringent filters at millimeter wavelengths was carried out at centimeter wavelengths, and it was thus demonstrated that birefringent filters can also be constructed and operated down to microwave frequencies. Here

they are equivalent to directional (nonreflecting) filters, and should be suitable for use in (higher-mode-free) beam waveguides, particularly at millimeter wavelengths.

The remainder of this section concerns certain elementary aspects of birefringent plates and filters as they apply here. Section II discusses considerations leading to the choice of a suitable artificial birefringent medium for the construction of a filter, and also the design and construction of the first test plate. In Sec. III, test results and theory for a five-element filter are compared, and the effect of the coarse structure of the artificial birefringent medium on the filter response is computed and compared with an ideal linear medium for a four- and a five-element filter. Analysis and synthesis methods, including the method of synthesizing birefringent filters with equal-ripple stop-band response, are described in Sec. IV. Design tables for optimum birefringent filters are presented in Sec. V, together with a description of their use.

B. THE BIREFRINGENT FILTER

The birefringent filter is a four-port, intrinsically reflectionless passive device. The term intrinsic is used because each element of the filter by itself is assumed to be ideally reflectionless. In practice, the elements can be well-matched over a broad band. The filter causes radiant energy entering one of the ports to separate into bands which emerge from two other ports, with no power emerging from the fourth port. This mode of operation is similar to that of a directional filter in microwave technology and is different from conventional reflection-type filters. The four "ports" are simply the two orthogonal polarizations of a plane wave at the input and output ends of a birefringent filter. The wave polarization is partially rotated as it passes through the filter, the amount of rotation depending on the wavelength. The power is always divided between the output ports; at certain discrete frequencies, all the power emerges from one port. Such wave rotation also occurs in each filter element; however, while all filter elements (plates) respond to a plane wave in a fundamentally similar way, a complete filter (cascade of

several crystals) can have a variety of different responses. For a multielement filter, the response depends on the following design parameters: (1) the length of a plate, (2) its birefringence (differential phase shift per unit length for the two polarization, which is a function of frequency); (3) the angles between the plate axes and the input polarization; and (4) the choice of output port (angle of output polarizer). This topic is discussed more fully in Sec. IV. Parts C and D of this section discuss the frequency response of a single plate, and the action of cascaded plates at one particular frequency, the design center frequency f_0.

C. THE BIREFRINGENT PLATE (FILTER COMPONENT ELEMENT)

1. General Properties Required for Filter Work

The term birefringence means double refraction as applied to an unpolarized beam of light striking the surface of an anisotropic crystal. As a result of the difference in refractive index for rays polarized normal and parallel to the optic axis, the beam is generally (but not always) split into two separate beams traveling in different directions inside the plate, as shown in Fig. 1. The condition under which no beam splitting occurs is precisely that required for birefringent filters. This situation is shown in Fig. 2. There, the input and output surfaces of the plate are parallel to the optic axis; propagation is normal to that axis, and of course to the two surfaces. Birefringence is then understood to be a differential retardation or phase shift between waves polarized normal to and parallel to the optic axis. In this report, the reference axis will be a direction normal to the optic axis rather than the optic axis itself. Here the optic axis is also called the fast axis (of polarization), in conformance with the characteristics of the laminated dielectric sandwich type of artificial birefringent medium used in the filters described herein. Birefringence of this type is defined as negative. A positively birefringent crystal, on the other hand, has its slow axis in line with the optic axis. An array of parallel dielectric cylinders (as opposed to plates) would have positive birefringence. Both positive and negative types of optical birefringent crystals occur in nature, and both types of birefringence can be realized at millimeter wavelengths.

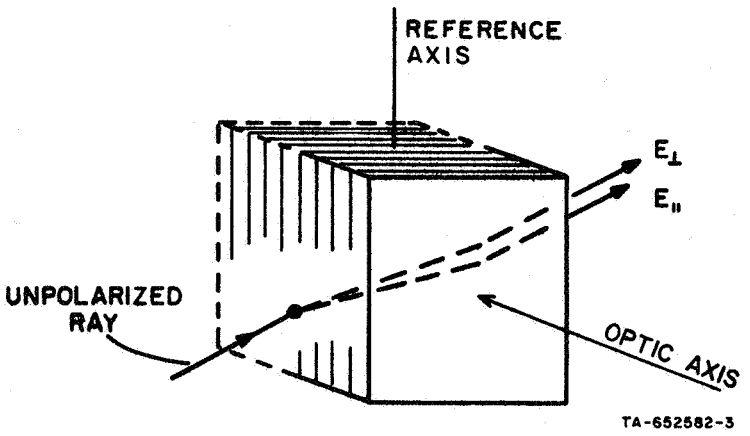

FIG. 1 OPTICAL BIREFRINGENCE — AN UNPOLARIZED RAY OF LIGHT IS SPLIT INTO TWO LINEARLY POLARIZED RAYS

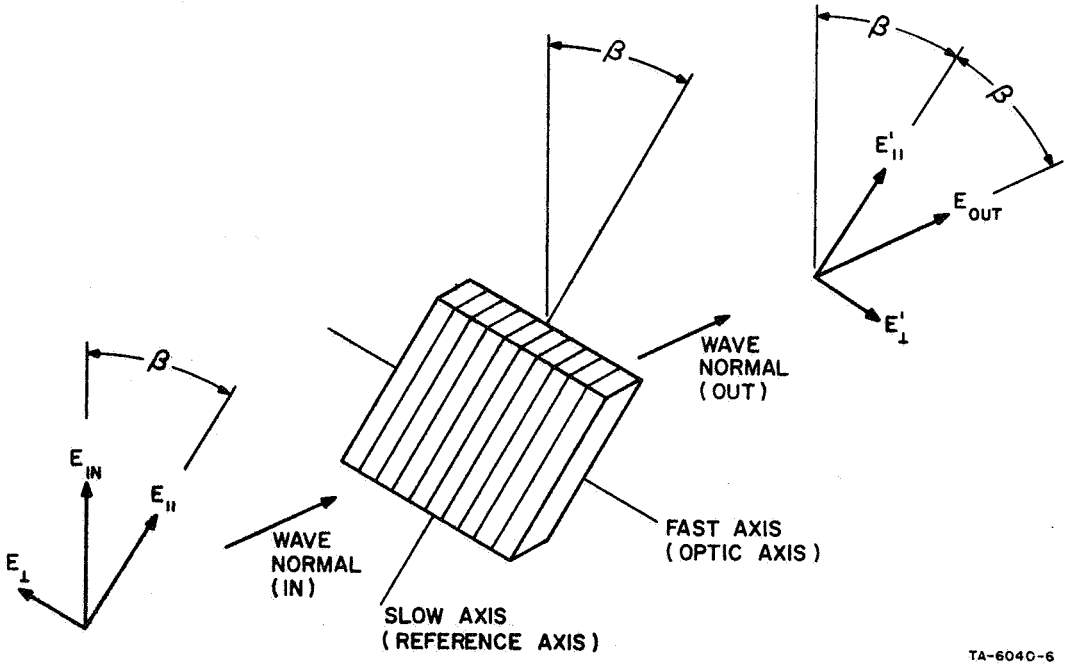

FIG. 2 EFFECT OF A BIREFRINGENT "HALF-WAVE PLATE" ON A LINEARLY POLARIZED INPUT WAVE

2. The Half-Wave Plate; Cascades of Half-Wave Plates

Figure 2 shows a birefringent plate that we will assume is impendance-matched to free space. We further assume that the frequency is such that linearly polarized waves normal and parallel to the plate reference axis suffer a differential phase change of 180 degrees. This frequency is called f_0, the design center frequency, and the crystal, at frequency f_0, is called a "half-wave plate." The following brief analysis of the action of a half-wave plate on a linearly polarized wave will yield a basic principle relating to the construction of birefringent filters.

An input wave with linear polarization in the vertical plane enters the crystal, the reference axis of which is at an angle β to the plane of polarization, and the output wave emerges on the right. As shown in Fig. 2, the input wave of amplitude E_{IN} is decomposed into its two components $E_\perp$ and $E_{||}$, which are, respectively, normal and parallel to the crystal reference axis. These waves $E_\perp$ and $E_{||}$ pass through the crystal without changing their amplitudes or direction of polarization and suffer a differential phase shift of 180 degrees. (The <u>total</u> phase shift of each wave is of no concern here, since it plays no part in the analysis.) Thus, to simplify the analysis, the phase of the emerging wave $E'_{||}$ is here chosen as zero degrees. The orthogonal wave, having traveled along the fast axis, will have suffered a relative phase advance of 180 degrees. Therefore, at the output, $E'_\perp$ may be depicted as a wave vector in phase with $E'_{||}$, but with its direction of polarization reversed 180 degrees in space with respect to $E_\perp$ at the input, as shown in Fig. 2. The two waves $E'_\perp$ and $E'_{||}$ (which are in phase in time) may now be added vectorially to form a linearly polarized wave, E_{OUT}.

The important point of this analysis is that the output wave now is at an angle β to the plate axis. Stated in another way, a rotation of the axis of a half-wave plate by an angle β from the plane of polarization of the incoming wave causes the plane of polarization of that wave to be rotated by an angle 2β. Thus, the horizontal and vertical components of the output wave are

$$E_V = E_{IN} \cos 2\beta \qquad (1)$$

and

$$E_H = E_{IN} \sin 2\beta \quad . \qquad (2)$$

When β = 45 degrees, it is seen that the half-wave plate can become a one-element filter, because all power at frequency f_0 emerges as a horizontally polarized wave ($E_V = 0$, $E_H = 1$).

When there are two plates, the first plate at an angle of β_1 degrees to the vertical, the wave entering the second plate (at frequency f_0) will be polarized at an angle of $2\beta_1$ degrees. Clearly, to emerge with horizontal polarization ($\beta_p = \pm 90$ degrees), the wave must be rotated by the second plate by the difference angle of $(\pm 90 - 2\beta_1)$ degrees. This rotation can be effected by letting the second plate be oriented at an angle β_2, such that the plate reference axis bisects the difference angle $(\pm 90 - 2\beta_1$ degrees). Thus,

$$\beta_2 = 2\beta_1 + \frac{1}{2} (\pm 90 - 2\beta_1) \text{ degrees} \quad . \qquad (3)$$

We can also write $\beta_2 = 2\beta_1 + \rho_p$,

where ρ_p is the output polarizer difference angle defined by $\rho_p = \beta_p - \beta_2$. Hence, ρ_p must also have the value

$$\rho_p = 1/2(\pm 90 - 2\beta_1) \quad . \qquad (4)$$

When the second plate is oriented at angle β_2, given by Eq. (3), the plane of polarization of the output wave is rotated exactly 90 degrees from the plane of polarization at the input. Equation (3) can be put in the following form,

$$\beta_2 - \beta_1 = \pm 45 \text{ degrees} \quad , \qquad (5)$$

which is the general solution for the two-plate filter. Although Eq. (5) guarantees that all power at f_0 emerges with horizontal polarization, it says nothing about the response at other frequencies, which of course depends on the choice of β_1 and the sign on the right-hand side of

Eq. (5). Nevertheless, a similar rather simple scheme can be used to design a filter at frequency f_0 with any number of plates, and with the total power output at any desired angle of polarization. To control the response at other frequencies as well, a more sophisticated approach is needed.

D. FREQUENCY RESPONSE OF A ONE-PLATE FILTER

Consider now the complete frequency response of a single-plate filter with unit input. Instead of a frequency variable f, we will use the birefringence parameter γ, which is one-half the differential phase shift of the plate. Here, γ will be assumed to vary linearly with frequency. Although this condition is generally not exact (it is an asymptotic condition for artificial anisotropic dielectrics at sufficiently low frequencies), the assumption of linearity is extremely useful in understanding birefringent networks. We thus define γ, for the present purpose only, as

$$\gamma = \pi f/2f_0 \quad . \tag{6}$$

The frequency response of the single-element filter is given by

$$E_V = \cos \gamma \tag{7}$$

and

$$E_H = j \sin \gamma \quad . \tag{8}$$

The derivation method for these formulas will be left for a later section; it suffices to say here that Eqs. (6) through (8) are based on an assumption that at f_0, the fast axis advances the phase by 90 degrees whereas the slow axis retards the phase by the same amount--all referred to some output reference phase which these equations state is zero.* The plate

---

* Physically, the rate of change of phase with frequency is proportional to time delay and must be positive. There is no similar restriction on phase, and the initial value of phase is like a constant of integration that may be assigned an arbitrary value, conveniently zero.

angle is assumed to be $\beta = 45$ degrees. According to Eqs. (6) through (8), the filter has two complementary outputs, and both are periodic in γ, with a period of 2π radians that encompasses two complete passbands and stopbands. One or the other output (either E_V or E_H) may be absorbed by a dummy load that permits only the desired signal to pass. This was accomplished by placing very thin parallel absorbing strips in the test horns and aligning them normal to the desired component. Note that E_V is unity and E_H is zero at $\gamma = 0$ (zero frequency). Thus, the direct (E_V) output has a low-pass filter form which is limited on the low-frequency end only by the size of the aperture, while either output could serve as a band-pass or band-stop filter, with center frequencies easily found from Eqs. (7) and (8).

E. ARTIFICIAL BIREFRINGENT MEDIUM

The construction of a birefringent filter for millimeter waves requires an artificial birefringent crystal or medium. Our choice was the air-dielectric sandwich, which has been analyzed by R. E. Collin.[10] Collin's second-order theory of birefringence in an air-dielectric sandwich material enables us to predict how the birefringence-vs-frequency function deviates from linearity and helps us to choose suitable dimensions for the filter structure.

II DESIGN OF AN ARTIFICIAL BIREFRINGENT PLATE

A. THE ANISOTROPIC MEDIUM

The first task was to construct a single birefringent plate which could later become one element of a multielement filter. Rough plate dimensions were calculated, based in general on the equipment to be used in testing the filter and in particular on the cross section and extent of the radiant beam that could be generated. When this work was first planned, the availability of electronically swept signal generators up to and including K-band (but not beyond) suggested a center frequency of about 20 GHz. The test filter would thus be a scale model of a millimeter-wave filter. A pair of horn reflectors with aperture cross sections of approximately 8 by 8 inches appeared to be well-suited for transmitting and receiving test antennas. When the antennas were separated about four feet, it was found that the signal-to-noise ratio of the test signal provided enough dynamic range to measure $\sim$ 40-dB insertion loss. A test plate of a complete filter could then be placed between the two horns, one of which was made rotatable. The test beam was well-collimated and its cross section was found to be little greater than that of the antenna apertures. On that basis, it was decided to make the plate aperture 10 inches square, so that it would encompass the test beam, and to make its length not much greater than its width to minimize the effects of any beam divergence. An upper limit of about 3 inches was thus placed on the thickness of a single plate in a four-element filter.

The plate design problem was then considered from the standpoint of materials, processes, and physical (electromagnetic) constraints. Several possible configurations were considered for the artificial birefringent medium. These included air-dielectric sandwiches, gratings of parallel dielectric rods, and gratings of parallel metal wires or strips. Only the first configuration appeared to be amenable to impedance matching over very wide operating bands. The need for impedance matching

of each element was stated in the previous section. The wide operating bandwidth requirement results from the fact that for a given order of pass band, the bandwidth is approximately proportional to the number of elements. Figure 3 shows four possible response shapes. The lowest pass band, at frequency f_0, was chosen as the main pass band (the lower right sketch in Fig. 3), in order to keep the overall length of the filter reasonably short. The width of the pass band to the half-power points was computed from an approximate formula derived from one given by Solc[3] (also approximate) for filters with equal plate angles:

$$\Delta f/f_0 \doteq 1.2/Nk \quad . \tag{9}$$

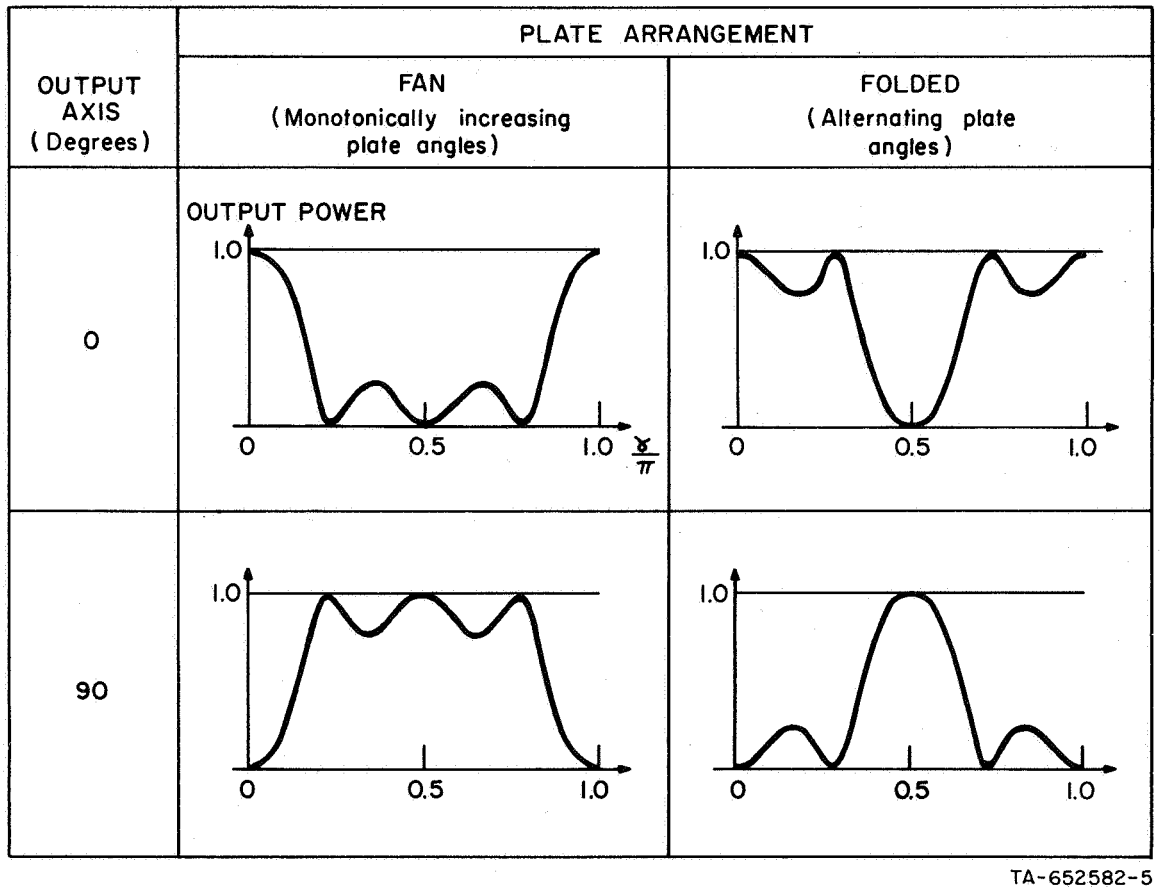

FIG. 3 FUNDAMENTAL PASS AND STOP BANDS OF EQUAL-LENGTH BIREFRINGENT FILTERS. (Two possible arrangements of plate angles and two polarizations of the output wave relative to the output wave relative to the input are shown.)

Here, N is the number of elements or plates and k is an integer representing the order of the pass band. (We choose k = 1 for the lowest-order non-zero pass band because this results in the shortest possible length for each plate, an important consideration here.) According to Eq. (9) for N = 4 and k = 1, we can expect pass bands of the order of 30 percent of the center frequency. It is thus clear that in order to measure both the pass band and the stop band, a wide operating band is required. Each plate would thus have to be matched by tapering or stepping the edges of the dielectric laminations. If a high-dielectric constant material were used for the plate laminations, a very compact filter could be provided. However, the high cost of such materials and the abrasive quality of the filler material (and consequent poor machinability) ruled out this choice in favor of Rexolite 1422 (relative dielectric constant $\varkappa_d = 2.53$), which has good machinability and dimensional stability, as well as low loss.

With the aid of Collin's[10] second-order theory of the birefringence of air-dielectric sandwich material, it was found that a plate thickness less than three inches was feasible, if Rexolite were used.

B. DESIGN OF A HALF-WAVE PLATE

The plan for plate construction, excluding framework, is shown in Fig. 4. Here, t is the maximum thickness of the dielectric material (Rexolite) and S is the spacing of the sheets of this material. In the tapered regions, which occupy two-thirds of the plate length (thickness), the sheet thickness t' varies linearly from 0 to t over more than a wavelength for both polarizations, yielding wide-band impedance matching. The normalized design parameters for the composite material are the ratios t/S for the inner region; t'/S (varying from 0 to t/S) in the two tapered regions; and S/λ, where λ is the wavelength in free space. The reference axis is parallel to the thin edge of a sheet of dielectric.

The most efficient use of the dielectric laminations is obtained when the ratio t/S is approximately 0.5. The birefringence for the static case is then near maximum for a given material. When frequency effects are considered, as in Collin's theory, the optimum ratio is a function of frequency and generally is less than 0.5. Excitation of grating

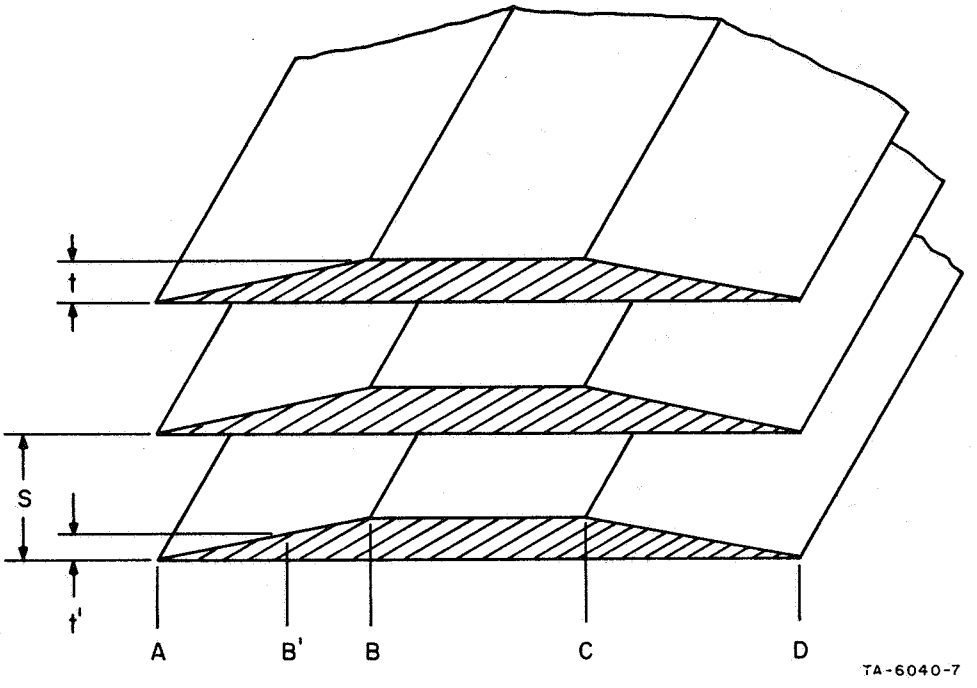

FIG. 4 SKETCH OF THE INTERNAL CONSTRUCTION OF AN IMPEDANCE-MATCHED ARTIFICIAL BIREFRINGENT PLATE

lobes will be prevented if S/λ_d is less than 1/2, where λ_d is the wavelength in the material of the dielectric sheets. With a relative dielectric constant of $\kappa_d = 2.53$ and a free-space wavelength of 0.59 inch (at $f_0 = 20$ GHz), we find that S/λ_0 should be no greater than 0.314. (This limitation on the lamination spacing was not adhered to, as explained below.) Also, in deciding on lamination thickness and spacing, the standard sheet thicknesses should be considered. In the range of interest, these are 0.125 and 0.063 inch. Since factory tolerances on sheet thickness are 0.004 inch for both sizes, the larger thickness gives greater accuracy in the ratios t/S and S/λ_0. In addition, half as many laminations would be required if the thicker sheet were used, and these laminations would be considerably more robust. The larger sheet thickness (t = 0.125 inch) was therefore chosen for the plate, and the value t/S was chosen as 0.4, which provided near-optimum efficiency, according to calculations based on Collin's theory. Combined, these values yield $S/\lambda_0 = 0.53$, a larger value than the 0.314 calculated above for the

maximum with respect to the generation of grating lobes. However, such lobing would normally be generated by discontinuities. Since the plan was to taper the laminations and thus essentially eliminate discontinuities, the high value of S/λ_0 was accepted in favor of the resulting more robust and easier-to-construct birefringent plate. An additional advantage of this choice was the fact that for the given range of test frequencies, the test data (by virtue of the scaling procedure) could be extrapolated to higher frequencies.

Collin's theory,[10] taking into account the effect of frequency on birefringence is given below. These formulas were used in determining the length of the plate, including the taper lengths. The formulas give the dielectric constants for the two polarizations; it is then a simple matter to determine the differential phase shift per unit length. We first give the static values of the dielectric constants of the composite material:

$$\varkappa_1 = \left[1 - \frac{\varkappa_d - 1}{\varkappa_d}\frac{t}{S}\right]^{-1} \tag{10}$$

and

$$\varkappa_2 = 1 + (\varkappa_d - 1)\frac{t}{S} \quad . \tag{11}$$

Here, $\varkappa_1$ is the static dielectric constant of the wave with E-field parallel to the reference axis (parallel to the plane of the laminations), and $\varkappa_2$ is the dielectric constant for the case of perpendicular polarization. The formulas for the second-order approximations of the dielectric constants are:

$$\varkappa_1' = \varkappa_1 + \frac{\left[(P_{11} + P_{00})^2 - 4\Delta\right]}{4\Delta P_{00}(2P_{00} - P_{11})}\frac{S^2}{\lambda_0^2} \tag{12}$$

and

$$\varkappa_2' = \varkappa_2 + \frac{(\varkappa_d - 1)^2}{16\pi^2}\left[32\sin^2\pi\frac{t}{S} + \sin^2 2\pi\frac{t}{S}\right]\frac{S^2}{\lambda_0^2} \quad , \tag{13}$$

where

$$\Delta = P_{00}P_{11} - P_{01}^2 \quad ,$$

$$P_{00} = 1 - \frac{\varkappa_d - 1}{\varkappa_d} \frac{t}{S} \quad ,$$

$$P_{01} = - \frac{\varkappa_d - 1}{\varkappa_d} \frac{\sqrt{2}}{\pi} \sin \pi \frac{t}{S} \quad ,$$

$$P_{11} = P_{00} - \frac{\varkappa_d - 1}{\varkappa_d} \frac{1}{2\varkappa} \sin 2\pi \frac{t}{S} \quad .$$

The formula for the total differential phase shift (2γ) of a uniform plate is

$$\gamma = \pi d(\sqrt{\varkappa_1'} - \sqrt{\varkappa_2'})/\lambda \text{ radians} \quad , \qquad (14)$$

where d is the length of a uniform (untapered) anisotropic plate. As an example of calculations of plate lengths by these second-order formulas, we find that for $d = \lambda = \lambda_0$, the differential phase shift <u>per free-space wavelength</u>, for the parameters adopted for the test plate in the uniform region, is 51.82 degrees at a value of $S/\lambda_0 = 0.53$ ($f_0 = 20$ GHz). (This compares with a <u>static</u> value of 44.8 degrees per free-space wavelength.) A uniform plate must then be slightly greater than 2 inches long to yield 180 degrees differential phase shift. A tapered plate would have to be somewhat longer, since the tapered portions contribute less to the total birefringence than the uniform portion.

The dimensions of a tapered lamination are given in Fig. 5. The length dimension was obtained as follows: The birefringence of the dielectric sandwich material was calculated for values of t/S and S/λ_0 from 0 to 1.0, in steps of 0.1. For the uniform region, where $t/S = 0.4$, the birefringence per free-space wavelength for $S/\lambda_0 = 0.53$ was found by interpolating between computed values of birefringence for S/λ_0 values of 0.5 and 0.6. Likewise, in the tapered region, where t'/S varied from

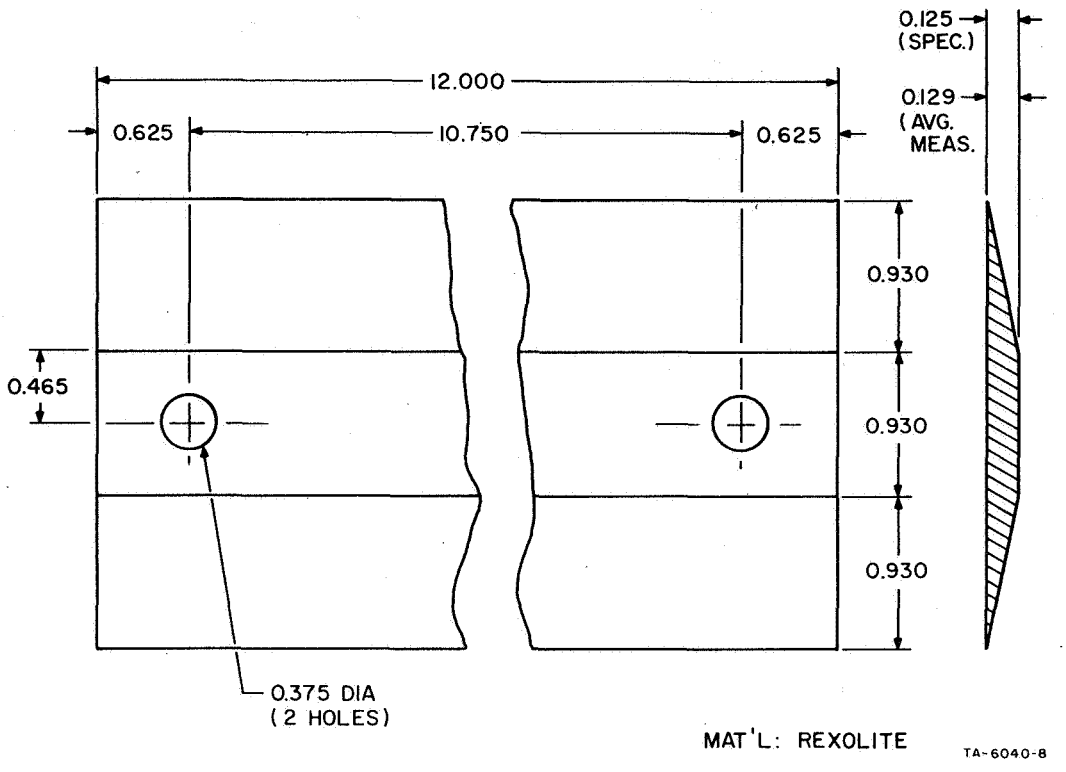

FIG. 5 SKETCH OF A PLATE LAMINATION, SHOWING DIMENSIONS

zero to 0.4, the birefringence of a single taper in terms of differential phase shift per free-space wavelength was calculated, using Simpson's rule. The birefringence of a complete plate with two tapered end portions equal in length to the central uniform portion was then computed by an averaging process. Thus, with two tapers yielding 31.16 degrees (computed) differential phase shift per free-space wavelength each, and a uniform portion yielding 51.82 degrees, we obtain an average of 38.04 degrees per wavelength at $\lambda = \lambda_0$. The overall required length is thus 180/38.04 = 4.73 wavelengths. With $\lambda = 0.59$ inch at $f_0 = 20$ GHz, we find the length to be 4.73 X 0.59 = 2.79 inches.

In the interest of brevity, the above description of the computation omits the method used to handle certain small details. These included the original use of $\kappa_d = 2.56$ rather than 2.53 (manufacturer's datum); the fact that the average lamination thickness was about 0.004 inch thicker than nominal, and corrections for these differences. A recomputation of

the center frequency of the plate, after it had been fabricated and after the above corrections had been made, yielded a center frequency of 19.85 GHz. (A later recalculation of the center frequency at the precise value of $S/\lambda_0 = 0.53$, rather than an interpolation from previously computed data, yielded $f_0 = 20.35$ GHz.)

The dimensions of each lamination are given in Fig. 5. A sketch of the front view of the plate is shown in Fig. 6. The laminations are separated by phenolic washers 0.194 inch thick. The plate frame is one-inch-thick phenolic laminate and is mounted on a rotatable sector of a circle 10.5 inches in radius, having its center at the center of the plate. The sector, in turn, is mounted on a large plywood base and can be clamped

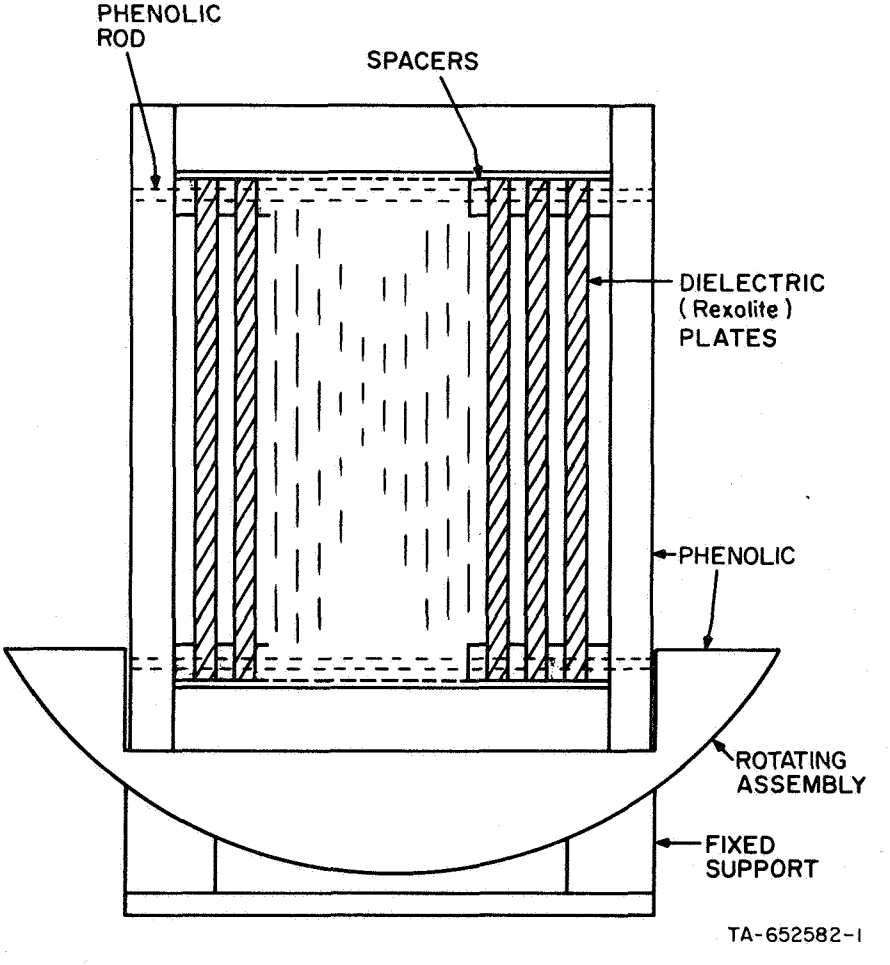

FIG. 6 FRONT VIEW OF A HALF-WAVE PLATE ASSEMBLY

into position at various angles to the vertical. A photo of the plate mounted on its base is shown in Fig. 7.

C. TEST RESULTS ON THE HALF-WAVE PLATE

The first half-wave plate was tested at the (originally) calculated center frequency of 19.85 GHz. The method of testing was to line up the test antennas in parallel (without the half-wave plate) so that a signal close to the maximum (which was made the reference level) was received. The half-wave plate was then inserted midway between the transmitting and receiving antennas, and its reference axis was varied from perfect parallelism with the plane of polarization of the incoming wave to a maximum angle of 45 degrees thereto in 5-degree steps. At each such position, the level of the received signal was noted, and compared with the reference level. The results are plotted as attenuation (dB) vs. orientation of plate (degrees) in Fig. 8. Two experimental curves of this characteristic, plus a theoretical curve based on Eq. (1) are given in Fig. 8. The lower experimental curve was obtained with the aid of a precision rotary attenuator, while the upper one was made by assuming perfect square-law operation of a crystal detector. The precision attenuator method presumably is more accurate than the crystal detector method; however, both are reasonably close to the theoretical curve, except in the region above plate orientations of 36 degrees.

In addition to testing the plate at the calculated value of f_0, tests were made to determine the actual center frequency. These yielded a center frequency $f_0 = 20.65$ GHz, with an estimated measurement accuracy of ± 0.15 GHz. (Later measurements on a filter composed of five identical plates gave $f_0 = 20.4$ GHz.)

In making the described measurements, it was necessary to fully absorb or divert (that is, reflect out of the system) the output wave orthogonal to the desired wave. Since the undesired component was horizontally polarized, plane gratings made of parallel thin wires spaced one-eighth inch apart were placed on each side of the test plate. The wires were horizontal, and the grating planes were at 45 degrees to the propagation path. The undesired component was thus reflected out of

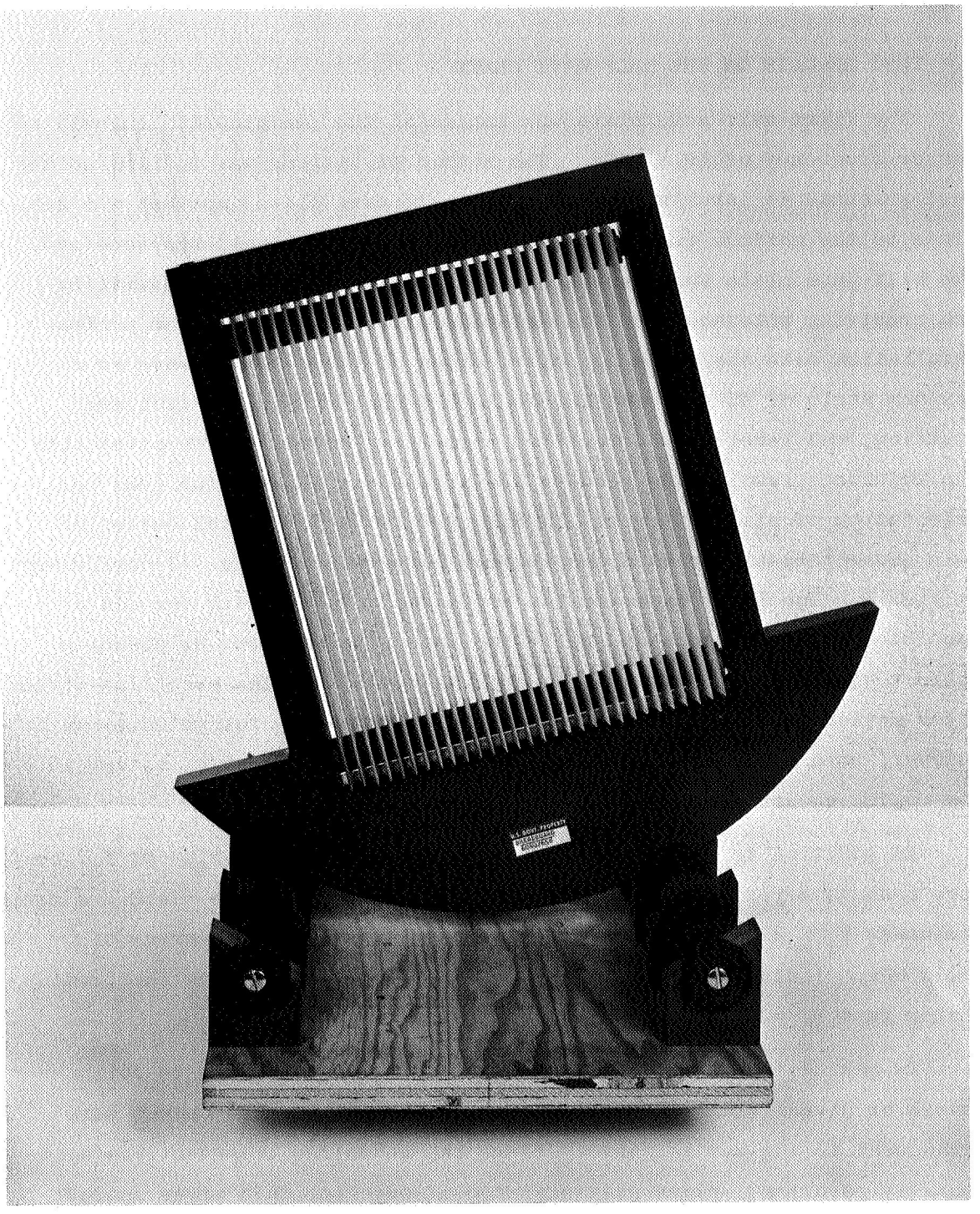

FIG. 7 PHOTOGRAPH OF A BIREFRINGENT HALF-WAVE PLATE ASSEMBLY, $f_0 \doteq 20$ GHz

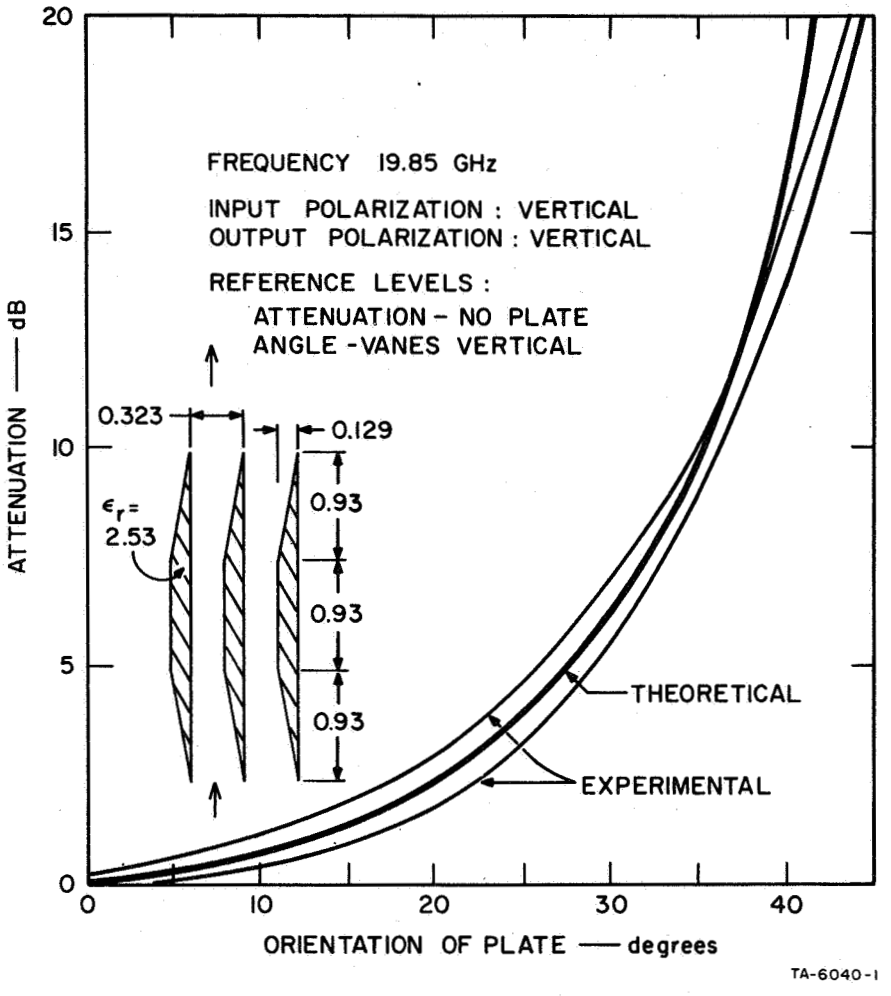

FIG. 8 THEORETICAL AND EXPERIMENTAL DIRECT-WAVE TRANSMISSION OF A LINEARLY POLARIZED BEAM THROUGH A HALF-WAVE PLATE FOR VARYING PLATE ANGLES. (The lower experimental curve was obtained with the aid of a precision attenuator; the upper curve was made by assuming a perfect-square-law crystal detector.)

the system, while the desired component was transmitted freely through the two gratings. Also, thin absorbent cards were placed inside each horn so that the desired component was transmitted freely and the undesired component was absorbed. These precautions were necessary to provide proper termination of all four (possible) ports of the network, the two input ports and the two output ports, as called for by theory. If this were not done, the undesired cross-polarized component would be reflected by the horns as in a Fabry-Perot resonator, ultimately entering the receive horn and disrupting the test measurements. The diverting gratings and the absorbing cards have the effect of severely dampening resonances of the undesired mode and thus preventing spurious responses of that type.

For this first test at f_0 on a single birefringent element, there appeared to be little or no reflections from the plate; the insertion loss was found to be very low, the measured center frequency was quite close to the design value, and the transmission-vs.-plate-angle characteristic was generally close to theoretical.

III DESIGN AND TEST OF A FIVE-ELEMENT FILTER

A. DESIGN

Once f_0 was chosen and the birefringent plate was designed, it remained only to choose the number N of plates to be cascaded and to determine the angles of orientation of each plate with respect to the input wave polarization. Solc[6] gave simple design formulas for filters with any value of N. These formulas were of two types: one in which the plate angles were arranged so as to tilt alternately, first on one side and then on the other side of the input polarization (this is called the folded-type filter), and one in which the plate angles increased monotonically in one direction (this is called the fan-type filter). The four possible responses of these two filter types are shown in Fig. 3. The upper row in Fig. 3 shows the responses of the filters when the received signal is polarized parallel to the input signal, and the lower row shows responses for the orthogonal wave. One can easily see that the lowest-center frequency, non-zero, narrow pass band occurs for a folded-type filter in the 90-degree output polarization, i.e., for the case illustrated in the lower right box of Fig. 3. The more plates used for the filter, the more ripples there will be in the stop-band regions on each side of the first pass band and, as indicated by Eq. (9), the narrower will be that pass band.

Solc's formulas for these two types of filter categorized by plate arrangement can be further classified as to sophistication of method of determining the actual plate angles. In the simpler class of filter, the absolute values of the difference angles between adjacent plates are equal and are identical for both the fan and the folded types, for the same value of N. The plate <u>difference angles</u> for the general filter of N plates are:

$$\rho_1 = \beta_1$$

$$\rho_2 = \beta_2 - \beta_1$$

$$\vdots$$

$$\rho_N = \beta_N - \beta_{N-1}$$

$$\rho_p = \beta_p - \beta_N \quad , \tag{15}$$

where the β_i are the plate angles as before, and β_p is the angle of the principal axis of the frame of reference for the output waves. The formulas for the plate angles of the folded type of filter are

$$\beta_i = \beta \quad , \quad (i \text{ odd})$$

$$\beta_i = -\beta \quad , \quad (i \text{ even}),$$

and

$$\beta_p = 90 \text{ degrees} \tag{16}$$

where

$$\beta = 45/N \text{ degrees} \quad . \tag{17}$$

The equations for the fan-type filter are given by:

$$\beta_i = (2i - 1)\beta, \quad (i = 1 \text{ to } N)$$

and

$$\beta_p = 0 \tag{18}$$

One may thus easily derive the design of one type of filter from the other. Furthermore, the response shapes will be identical except for a shift of one-half cycle in γ and a shift of the output arm to the one orthogonal thereto, as can be seen in Fig. 3. The ripples in the stop

band that are nearest to the pass band are generally quite severe in this type of filter, and for large values of N they are orders of magnitude greater than the lesser ripples. This undesirable situation can be ameliorated to a certain degree in Solc's second class of filter designs,[6] where the $|\beta_i|$ of Eq. (16) are not equal. In order to test an experimental filter, the first class (equal plate angles) was preferred as a design basis, since the larger stop-band ripples could be more easily measured and the equal-angle design could be more easily set up. Filter designs in which all stop-band ripples are equal in magnitude are discussed later in this report. At this point in the research, no such designs for birefringent filters were available.

Four additional plates identical to the first test plate were constructed so that a filter with up to five plates could be tested. The advantage of testing a five-plate filter over a four-plate filter, as originally planned, can be seen from Figs. 9 and 10. These two graphs are the calculated frequency responses of an equal-angle four- and five-element filter, respectively. In Fig. 9 the solid line shows the calculated frequency response using Collin's second-order theory[10] described in this report, for a set of alternating plate angles $\beta_i = \pm 11.25$ degrees in a four-element filter. (The method of calculating the response will be described later.) The solid line in Fig. 10 shows the response of a five-element equal-angle filter. In this case the plate angles are ± 9 degrees. One may note that the peak of the lower stop-band ripple for the four-element filter occurs slightly above 8 GHz, while in the five-element filter that peak occurs at about 11 GHz, making it much more observable in an X-band test setup. A similar situation holds for the first upper ripple in the upper stop band, so that the value N = 5 appears to be a better choice for testing an experimental birefringent filter.

In addition to aiding the selection of N, Figs. 9 and 10 show quite clearly how the nonlinear birefringence-vs.-frequency characteristic of the artificial dielectric medium causes a crowding of the pass bands and stop bands at the high-frequency end of the spectrum. A comparison between the filter responses for the ideal linear response medium and the

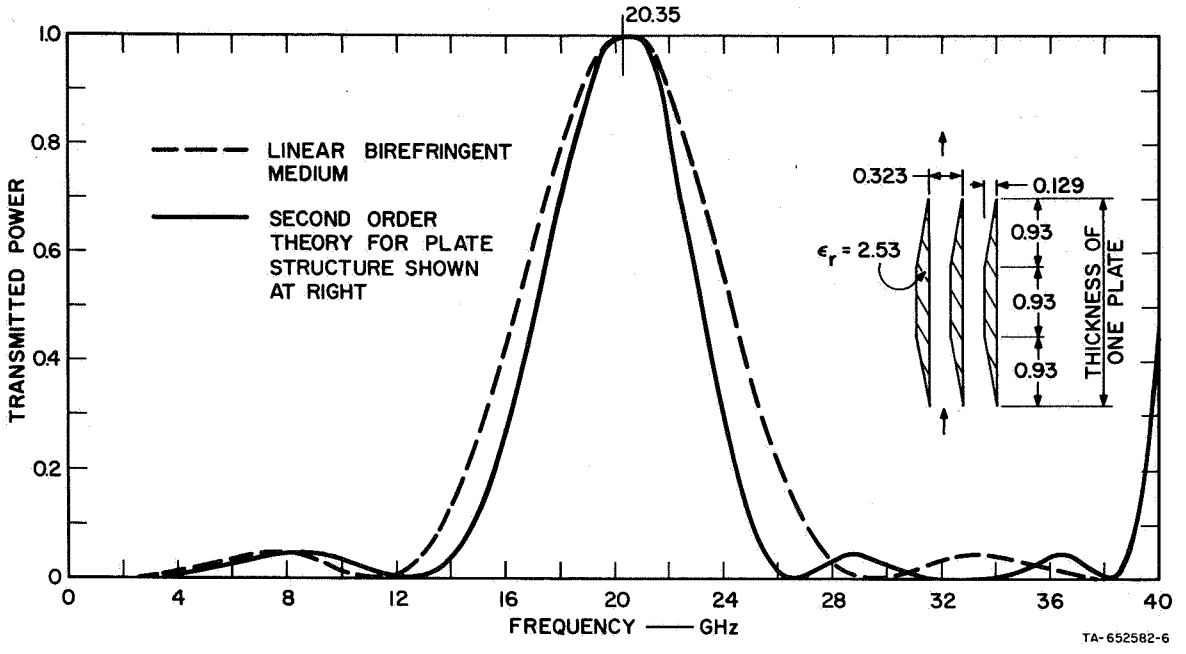

FIG. 9 COMPUTED RESPONSE OF AN EQUAL-LENGTH-PLATE, FOUR-ELEMENT, FOLDED-TYPE FILTER WITH PLATE ANGLES OF ±11.25 DEGREES
(The dashed line is for a linear birefringent medium; the solid line is for the structure shown.)

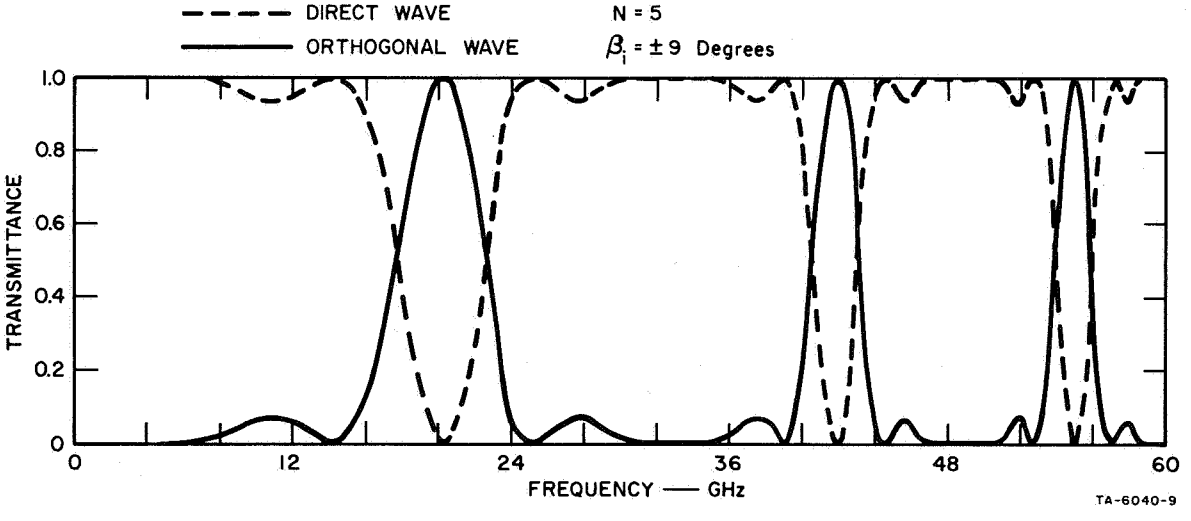

FIG. 10 COMPUTED AND RELATIVE POWER OF THE DIRECT AND ORTHOGONAL OUTPUTS OF A FIVE-ELEMENT EQUAL-ANGLE FILTER WITH THE FILTER-ELEMENT STRUCTURE OF FIG. 8

non-linear medium can be made in Fig. 9 by comparing the dashed line, representing a linear response, with the solid line. (The dashed line in Fig. 9 is for a linear filter assumed to be centered at f_0 = 20.35 GHz; it is not the calculated first-order response for the plate structure shown in the inset, which would have a higher center frequency than the f_0 of Fig. 9.)

The dashed line in Fig. 10 is the complementary output (absorbed component) of the five-element filter and is labeled "direct wave," since its E-field lies in the same plane as the input wave. It would appear that the stop-band ripples, other than those closest to the pass bands, are missing; however, this is only because their amplitude is imperceptible on the scale used in Fig. 10. These minor ripples are shown in some of the following figures. (There are actually two ripples in the lowest stop band--four in all the others of a five-element equal-angle filter.)

B. TEST

The five-element folded-type filter was tested, over the range of 8 to 33 GHz, first in the narrow-band (bandpass) mode, i.e., with the output taken from the orthogonal arm. The test results together with the calculated response (filter attenuation vs. frequency) are shown in Fig. 11. (The method used in calculating the response of birefringent filters is outlined in the next section.) Here, measurement accuracy depended on precision attenuators. Photographs of the assembled filter and the test setup are shown in Figs. 12 and 13, respectively. The experimental points plotted in Fig. 11 were obtained by two methods: In the frequency range above 22 GHz, the measurements were made at discrete frequencies; at lower frequencies, the frequency was swept electronically. The experimental points in the region below 22 GHz also include some point-by-point measurements as a further check. The reference levels were measured when the test horns were (polarized) parallel and the filter was absent from the path of transmission. The receive horn was then rotated 90 degrees, causing the received signal to be attenuated by about 40 dB or more, without the filter in position. The filter was subsequently inserted in the path of transmission and the signal level was again measured.

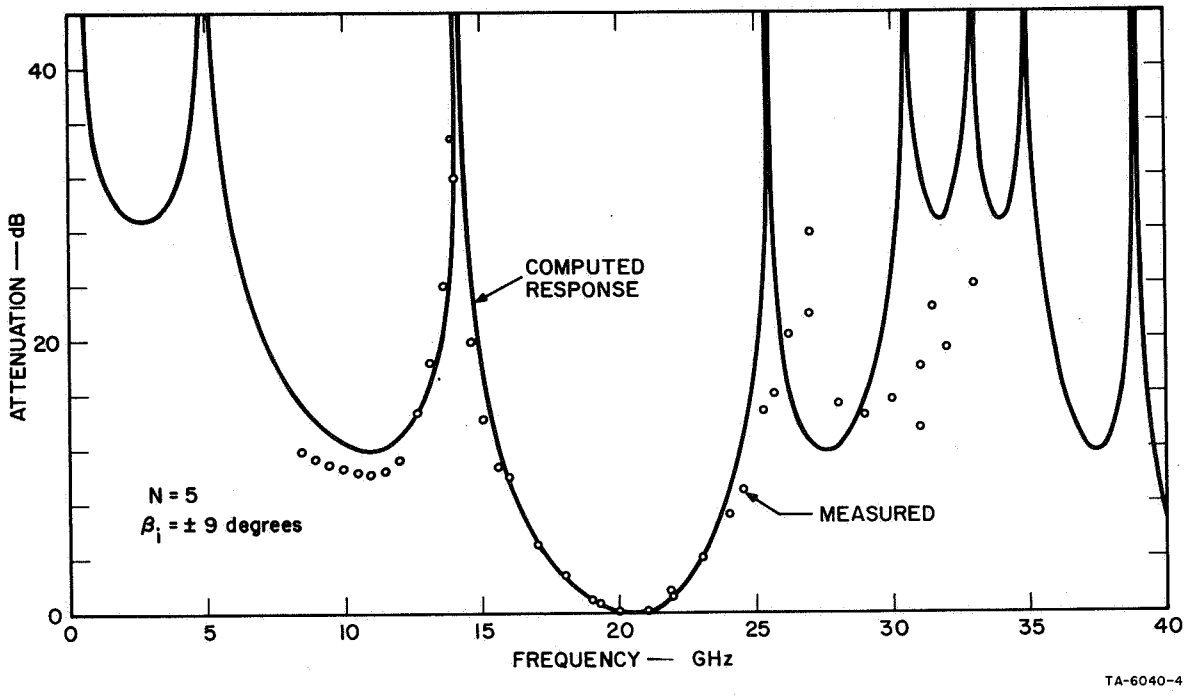

FIG. 11 MEASURED AND COMPUTED ATTENUATION RESPONSE OF THE ORTHOGONAL OUTPUT (NARROW-BAND) OF THE FIVE-ELEMENT EQUAL-ANGLE FILTER OF FIG. 12

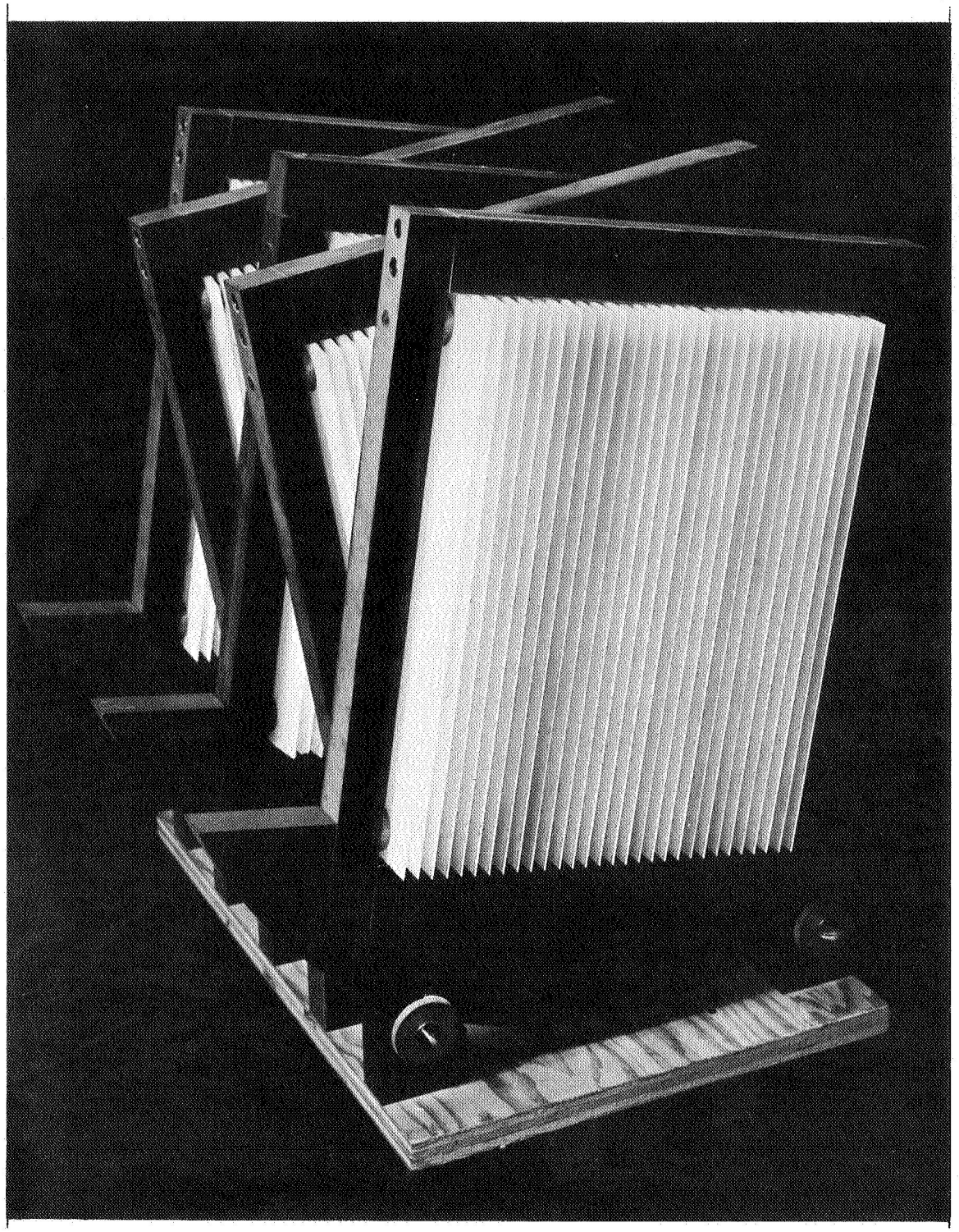

FIG. 12 PHOTOGRAPH OF THE EXPERIMENTAL FIVE-ELEMENT FILTER
(See Figs. 11 and 14 for measurements on this filter.)

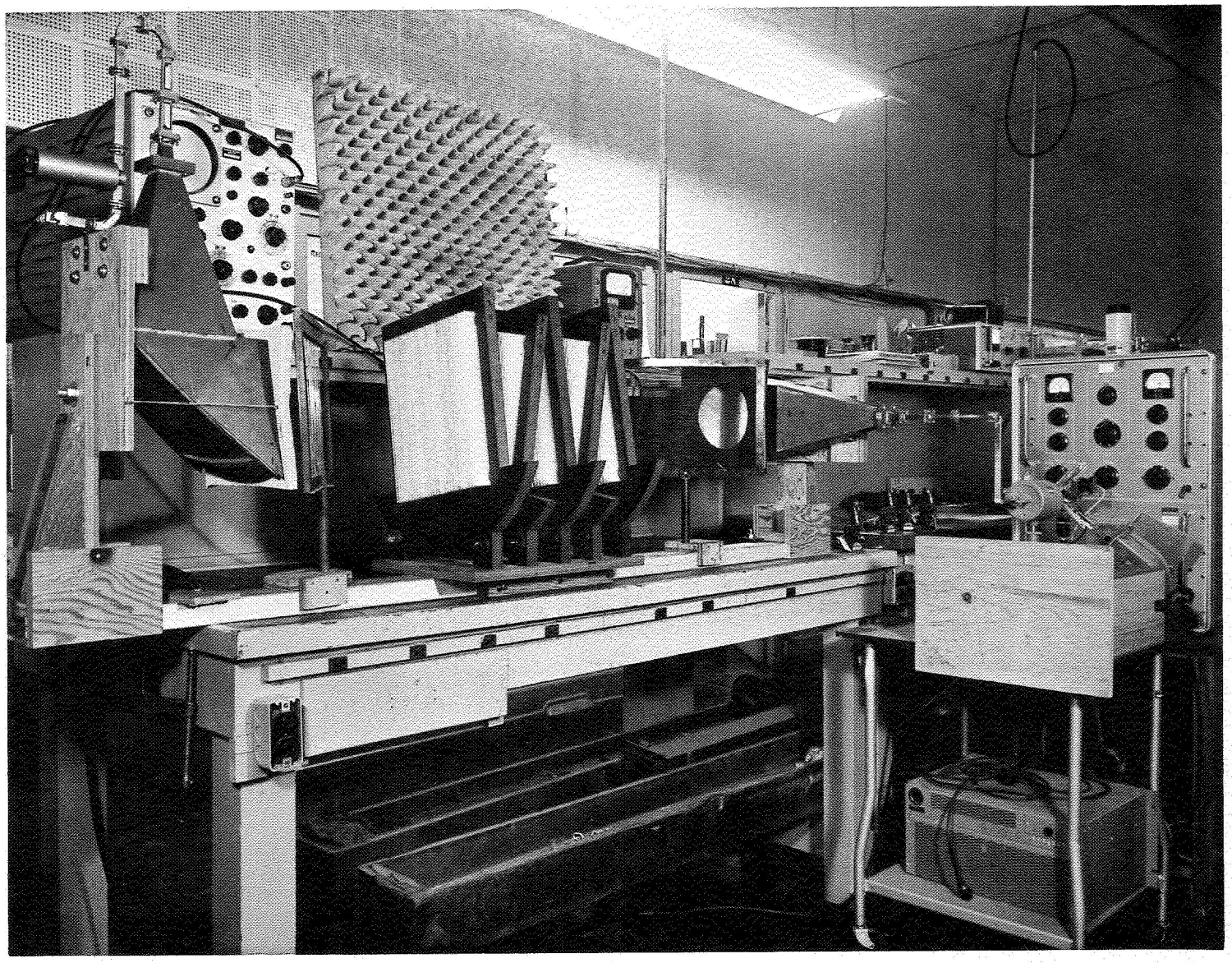

FIG. 13 PHOTOGRAPH OF THE INSTRUMENTATION USED FOR MEASURING THE ATTENUATION vs. FREQUENCY RESPONSE OF THE FILTER OF FIG. 12

A plot of the filter response for the bandstop mode is shown in Fig. 14 over the range 16 to 33 GHz. For reference purposes, the calculated theoretical responses of both modes are plotted on the same scale in Fig. 15; however, here the abscissa is the parameter γ, so that there is no crowding of the response shape in the upper part of the spectrum such as occurs when frequency is used as the independent variable (Figs. 11 and 14). The filter response shown in Fig. 14 was made with both antennas aligned parallel, and they remained so throughout the test; no rotation of the horn was required.

The test results (Figs. 11 and 14) tend to confirm the validity of Collin's second-order theory of the birefringence of artificial anisotropic dielectrics,[10] and Solc's theory with respect to equal-length birefringent filters.[6] Solc had, of course, constructed filters at optical frequencies, while the work at SRI was done at frequencies many orders of magnitude lower. Thus, instead of a filter diameter of many thousands of

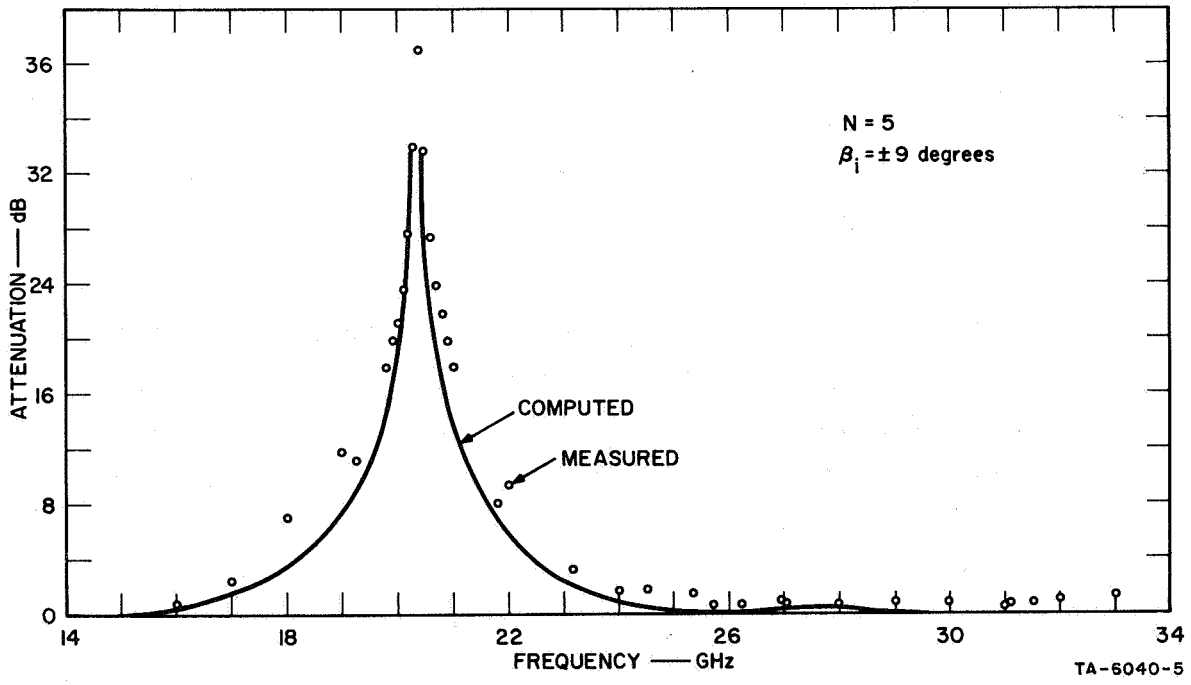

FIG. 14 MEASURED AND COMPUTED RESPONSE OF THE FILTER OF FIG. 12 FOR THE BANDSTOP MODE

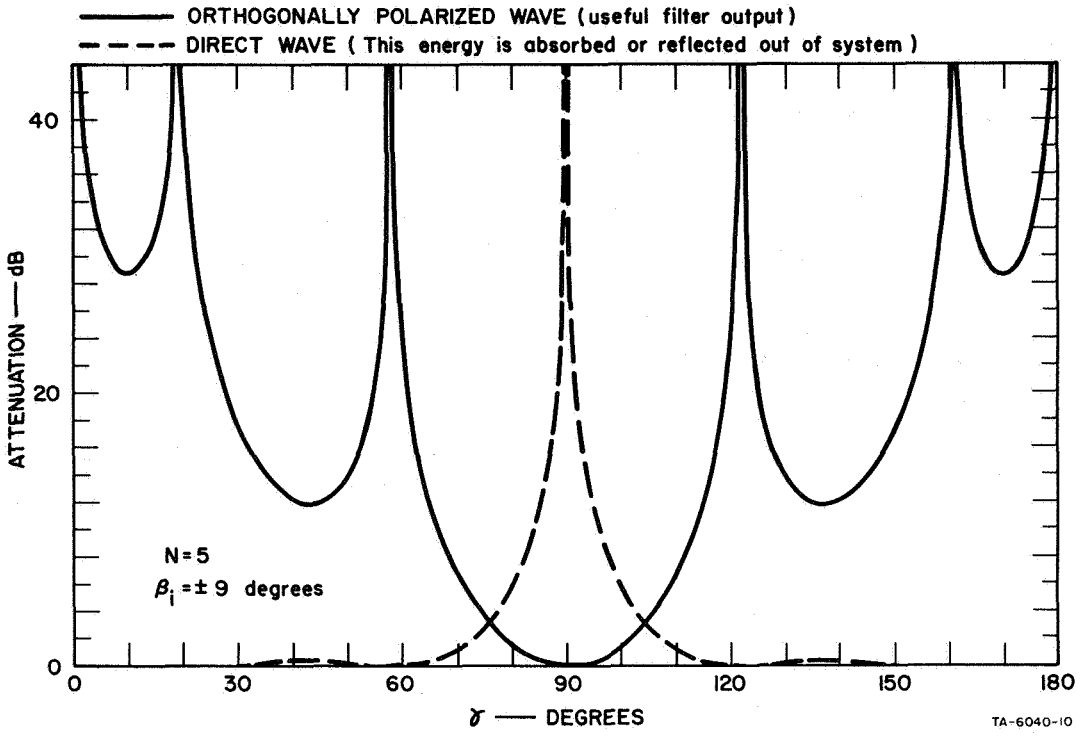

FIG. 15 COMPUTED ATTENUATION RESPONSE OF THE FIVE-ELEMENT EQUAL-ANGLE FILTER WITH γ AS THE INDEPENDENT VARIABLE

wavelengths, our filter is only about a dozen wavelengths across, and there are probably appreciable phase variations in the receive horn aperture.

It may be noted in Fig. 11 that the region of closest agreement between test measurements and calculated response lies in the range 13 to 24 GHz. Below this range it was found that the diameter of the test beam was noticeably larger than at the design frequency, and some of the radiated energy appeared to be in a position to be intercepted by the frames of the plates. This situation could have modified the filter response to some degree, by either guiding or focussing the beam. This supposition is supported by the fact that in the lower-frequency region, the measured response was consistently greater for both the narrow-band (bandpass) mode of Fig. 11 and the bandstop mode (this region is not shown on Fig. 14). In particular, for the bandstop mode a net pseudo-insertion gain of about 1 dB was measured, whereas the attenuation should have been near zero

decibels. This anomaly tends to support the belief that some energy from the transmit horn bypassed the receive horn, owing to natural spreading of the beam, and then, when the filter was inserted in the transmission path, it was redirected into the receive horn, where it interfered constructively in the receive horn aperture. It is more reasonable to attribute this pseudo-insertion gain effect to scattering by the plate frames, or to diffraction from the plate edges (similar to the focussing of a lens) than to an inherent quality of the artificial birefringent medium.

The deviation of the measured points from the computed line in the upper stopband (Fig. 11) may be attributed to one of two causes, or to a combination of both causes. First, we had difficulty in satisfactorily dampening resonant modes of the undesired (direct-wave) response during the course of the measurements in the upper stopband (Fig. 11). Some of this difficulty was caused by the fact that adjustments of wire gratings and absorbent cards were made at fixed frequencies, as were the measurements, so that there was always the possibility of hidden interactions which were canceled out during adjustment but which reappeared when the filter was inserted. Also, part of the difficulty may be attributable to the inaccuracies in the horn construction, which are more serious at the higher frequencies, especially when one considers that the horns were operating at about twice their original design frequency, Dispersion in the test measurements in the high-frequency region tend to support the above reasoning.

Second, it is quite possible that the energy distribution in the infinite medium postulated by Collin's theory does not occur in a finite-length plate for the large S/λ values used here, even when long portions of the plate are tapered. The first-measured near-null above the passband in Fig. 11 occurs at about 1 GHz above the computed null frequency, and the first-measured stop-band ripple appears to be somewhat spread out, as though there was a relaxation of the nonlinear second-order effect, in support of the above supposition.

IV ANALYSIS AND SYNTHESIS

A. ANALYSIS OF FILTERS WITH EQUAL-LENGTH PLATES

Evans[11] has described a method of calculating the response of birefringent filters composed of equal-length elements using a matrix multiplication technique attributed to Jones.[12]

A complex output wave vector $\bar{E}_{OUT}$ is found by premultiplying the input wave vector $\bar{E}_{IN}$ by a matrix [M] representing the birefringent filter:

$$\bar{E}_{OUT} = [M]\bar{E}_{IN} \quad . \tag{19}$$

The wave vectors are two-element column vectors and M is a 2-by-2 square matrix. Thus

$$\bar{E}_{OUT} = \begin{pmatrix} E_X \\ E_Y \end{pmatrix}^{*} \text{ and } \bar{E}_{IN} = \begin{pmatrix} E_V \\ E_H \end{pmatrix} \quad .$$

Expanding Eq. (19), we obtain

$$E_X = M_{11}E_V + M_{12}E_H \tag{20}$$

and

$$E_Y = M_{21}E_V + M_{22}E_H \quad . \tag{21}$$

For a vertically polarized input wave of unit amplitude ($E_V = 1$, $E_H = 0$) the output wave components are seen to be

$$E_X = M_{11} \qquad E_Y = M_{21} \quad . \tag{22}$$

---

* The X-Y and V-H axes are independent, with the X-axis at an angle β_p to the V-axis.

It now remains to specify the components of the filter matrix [M], which is the product of plate matrices [P] and rotation matrices [S]. First, the matrix for a plate is given by

$$[P] = \begin{pmatrix} e^{j\gamma} & 0 \\ 0 & e^{-j\gamma} \end{pmatrix} , \tag{23}$$

where, as before, 2γ is the differential phase shift of the two orthogonal waves on the principal axes of the plate. The matrix for a rotation by an angle β is

$$[S(\beta)] = \begin{pmatrix} \cos\beta & -\sin\beta \\ \sin\beta & \cos\beta \end{pmatrix} . \tag{24}$$

The [S] matrix rotates the wave vector and plate (as a system) so that the plate axis is aligned with the vertical axis, and then rotates them back again to the original angle, so that the vertical and horizontal complex components of the output vector are obtained. This is done for a single plate through a combination of pre-multiplication and post-multiplication by the [S] matrix as follows:

$$\bar{E}_{OUT} = [S(\beta)][P][S(-\beta)]\bar{E}_{IN} . \tag{25}$$

For several plates we obtain a chain matrix, which--after a simple substitution--can be put in the following form:

$$\bar{E}_{OUT} = [S(-\rho_p)][P][S(-\rho_N)][P][S(-\rho_{N-1})][P]\ldots$$
$$[S(-\rho_2)][P][S(-\rho_1)]\bar{E}_{IN} . \tag{26}$$

Here the ρ_i are as defined in Eq. (15). Equation (26) is easily programmed, and it has been used to compute filter responses. Since the independent variable in the [P] matrix is γ, the frequency response of the filter

was obtained by substituting frequency values corresponding to values of γ used in the filter response calculations. A curve showing the needed relationship had been calculated by Eqs. (10) to (14) for the specific plate structure of the filter and was used here. Later, the two programs were combined so that frequency was the independent variable and frequency response was given directly by the computer.

B. SYNTHESIS OF OPTIMUM RESPONSE FILTERS

1. General

Harris et al described a general procedure[7]* for the synthesis of lossless birefringent networks. In the referenced article, an example of an optical discriminator designed using this theory and a full description of the physical limitations on the response shape are given. Basically, these are governed by the conservation of energy (the total power in both output arms shall be equal to the input power) and the stipulation that there shall be no more conditions placed on the specific shape of the response than there are degrees of freedom in choosing the plate angles and the angle of the output horn or polarizer. Thus, in an N-plate filter there are (N + 1) allowed degrees of freedom.

Before the synthesis procedure can begin, a Fourier series representation of the desired response must be found. Now, the standard Fourier series method leads to a least-mean-square approximation of zero response in the stop band with accompanying large amplitude ripples near the pass-band edge, a condition known as Gibbs' phenomenon. Furthermore, the stop-band ripples are grossly unequal (also true of Solc's filter designs), which is precisely the situation one attempts to avoid in filter design work. Dolph's[13] method of designing antenna arrays with equal-amplitude sidelobes includes a method of obtaining a Fourier series with equal-amplitude ripples. His method is employed here as a preliminary step in the synthesis procedure proper; then the Harris method[7] is used to obtain birefringent filters with equal-amplitude stop-band ripples. The Dolph

---

* This shall be known throughout the report as the "Harris" procedure or method.

method will be illustrated for the case of N = 5 up to the point of obtaining formulas for coefficients of the Fourier series after which, Harris's procedure is required. Following that, iterative procedures good for any value of N will be given and the method of obtaining them will be discussed.

Let us first consider the mathematical form of the response [M_{11} of Eqs. (20) and (22)] of equal-length, lossless birefringent filters. If the components of M_{11} are found by multiplying out Eq. (26) for a specific value of N, one obtains sums of exponential terms in the variable γ, with coefficients that are functions of the plate difference angels ρ_i, including ρ_p. We shall use the ρ_p of Eqs. (15), (16), and (18), and be concerned only with folded and fan-type filters that have their plates symmetrically or antimetrically disposed about certain axes on the central plane of the filter: the vertical axis for the folded type, and a 45-degree line for the fan type. It can then be shown that the term M_{11} can be put in the form of a Fourier cosine or sine series. For the fan-type filter, with N even,

$$M_{11} = A_0 + \sum_{k=2}^{N} A_k \cos(k\gamma) \qquad (k \text{ is even}) \quad , \tag{27}$$

and with N odd,

$$M_{11} = \sum_{1}^{N} A_k \cos(k\gamma) \qquad (k \text{ is odd}) \quad . \tag{28}$$

For the folded-type filter, with N even,

$$M_{11} = j\left[\sum_{k=2}^{N} A_k \sin(k\gamma)\right] \qquad (k \text{ is even}) \quad , \tag{29}$$

and with N odd,

$$M_{11} = j\left[\sum_{1}^{N} A_k \sin(k\gamma)\right] \qquad (k \text{ is odd}) \quad . \tag{30}$$

The expressions for the M_{21} outputs for the two types of filter are more complex than Eqs. (27) through (30), and the latter equations are more suitable for the approximation procedure. The one used in this report is Eq. (28), which is a Fourier cosine series with only odd terms, corresponding to the direct output of a fan-type filter with N odd. A fan-type filter will thus be directly synthesized; however, as mentioned earlier, the analogous folded-type design can be easily obtained from the fan-type design; in fact, the tables of Sec. V reflect this procedure. In respect to the above discussion on symmetrically arranged plates and the resulting mathematical form of the response functions, we may also note the following: Mertz[14] and Harris[7] showed that the frequency response of lossless, impedance-matched birefringent filters must be of the form of a finite Fourier exponential series. If one further requires that the response be symmetrical or antimetrical about $\gamma = \pi/2$, then only odd or only even terms appear in the series, so that it can be converted to a Fourier sine or cosine series as in Eqs. (27) through (30). This suggests that the synthesized optimum response filter will have a symmetrical or antimetrical arrangement of the plate angles, which is indeed the case. The symmetry relationships that were discussed briefly here are fully explained in an article by Ammann[15] on the general properties of birefringent networks.

2. Finding the Fourier Series (N = 5)

Dolph's[13] design method as applied to our problem is to take the coefficients of an equal-ripple Chebyshev polynomial term by term and make them the coefficients of a polynomial in the variable $(\cos \gamma)$. The latter is then a power series in $(\cos \gamma)$* with the same equal-ripple behavior as the Chebyshev polynomial; however, because of the periodic behavior of the cosine function, this power series is also periodic, and of course, unlike a Chebyshev polynomial, it is always finite. The power series is then rewritten in the form of a Fourier series, as

* Part of the Chebyshev function is discarded in this process.

required for the Harris synthesis procedure. Two scaling procedures must also be used. These will be done before the substitution of variables, described above, is made.

We start with a Chebyshev polynomial of order 5, sketched in Fig. 16:

$$T_5(y) = 16y^5 - 20y^3 + 5y \quad , \tag{31}$$

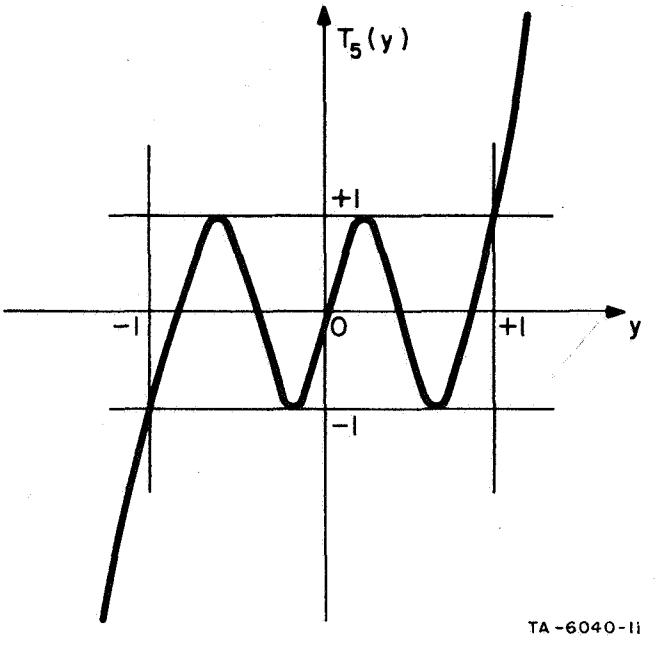

FIG. 16 SKETCH OF THE ESSENTIAL CHARACTER OF A CHEBYSHEV POLYNOMIAL OF THE FIRST KIND, OF ORDER 5

where $T_5(y)$ is an odd polynomial with equal ripples of maximum amplitude ± 1 in the interval $-1 < y < +1$. Outside this range, $T_5(y)$ increases in the negative or positive direction monotonically. The ripples correspond to the low-amplitude response ripples in the stop band of the birefringent filter, hence we must add a scale factor to the polynomial and thereby reduce the ripples to the desired value, say $\epsilon < 1$. This is done by multiplying the polynomial by ϵ, which will give another equal-ripple polynomial, as follows:

$$P_5(y,\epsilon) = \epsilon T_5(y) = \epsilon(16y^5 - 20y^3 + 5y) \quad . \tag{32}$$

The ripples in P_5 now have a maximum amplitude of $\pm\epsilon$. The second scaling procedure has to do with determining how much of the original Chebyshev polynomial is to be discarded and how much retained in a specific design. Note that since the entire equal-ripple portion of P_5 corresponds with the stop band, a portion of the monotonic region of that function must be retained for the pass band and the remainder discarded. This is done by replacing the variable y by y/y_1, where $y_1 < 1$. The two scaling procedures yield

$$P_5\left(\frac{y}{y_1},\epsilon\right) = \epsilon T_5\left(\frac{y}{y_1}\right)$$

$$= \epsilon\left(16\frac{y^5}{y_1^5} - 20\frac{y^3}{y_1^3} + 5\frac{y}{y_1}\right) \quad , \tag{33}$$

which is sketched in Fig. 17. The constant y_1 corresponds with the edge of the stop band in the Fourier-series representation. Since the Chebyshev

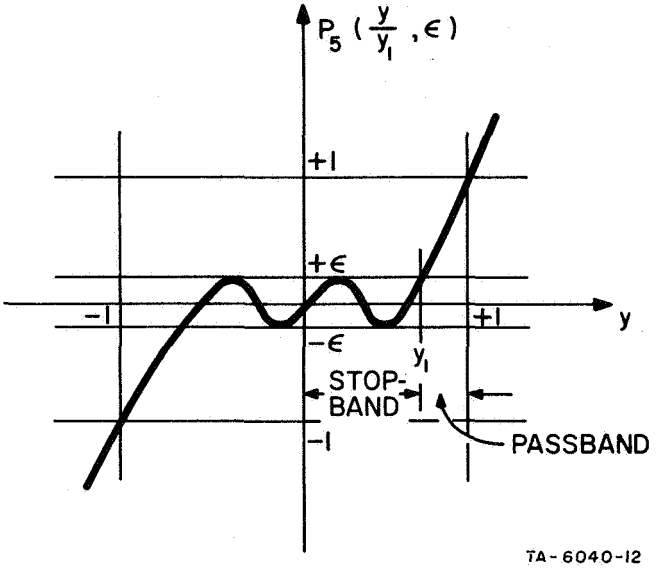

FIG. 17 THE SCALED CHEBYSHEV POLYNOMIAL OF ORDER 5

polynomials always take on the values ±1 at y = 1, $P_5(y/y_1,\epsilon)$ always takes on the values ±ε at $y = y_1$, as can be easily ascertained from Eq. (33).

We next make the substitution

$$\cos\gamma = y \quad , \tag{34}$$

which yields a power series in the variable cos γ. We now have

$$P_5\left(\frac{\cos\gamma}{y_1}, \epsilon\right) = \frac{16\epsilon}{y_1^5}\cos^5\gamma - \frac{20\epsilon}{y_1^3}\cos^3\gamma + \frac{5\epsilon}{y_1}\cos\gamma \quad . \tag{35}$$

It should be noted that the use of the cosine substitution [Eq. (34)] reverses the response shape from left to right when γ (not cos γ) is the independent variable, so that the pass band is centered on γ = 0, as is required for the fan type of filter. One more step is needed before Eq. (35) can represent the normalized response of a filter with zero loss at band center. We must insure that $P_5(\cos\gamma/y_1, \epsilon) = 1.0$ at γ = 0, as sketched in Fig. 18, for zero loss at band center. This is done by fixing the relationship between ε and y_1. First, γ is set equal to zero; then, after equating the right-hand side of Eq. (35) to 1.0, we solve for ε in terms of y_1:

$$\epsilon^{-1} = \frac{16}{y_1^5} - \frac{20}{y_1^3} + \frac{5}{y_1} \quad . \tag{36}$$

---

* We can also solve explicitly for y_1 using Eq. (39):

$$y_1^{-1} = \cosh\frac{1}{5}\cosh^{-1}\frac{1}{\epsilon}$$

Here, $y_1^{-1} > 1$, hence cosh is substituted for cos in Eq. (39).

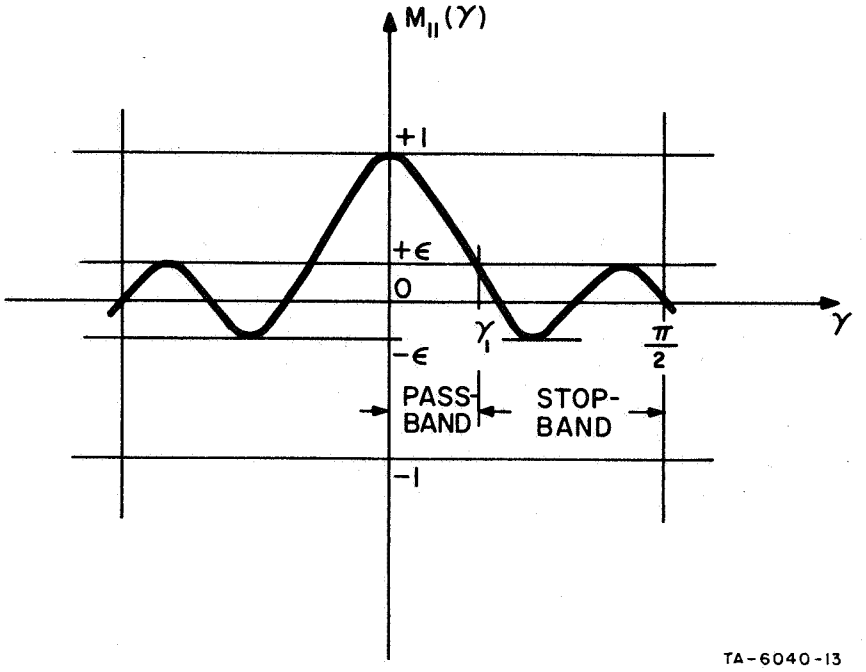

FIG. 18 SKETCH OF THE ESSENTIAL CHARACTER OF A FOURIER COSINE SERIES OF ORDER 5 DERIVED FROM THE SCALED CHEBYSHEV POLYNOMIAL. (This is also the M_{11} term of the matrix for the output waves of a fan-type, five-element, equal-ripple response filter when the average time delay is assumed to be zero.)

From Eq. (34),

$$\cos \gamma_1 = y_1 \quad , \tag{37}$$

and γ_1 is seen to be the edge of the stop band in the variable γ. Once the edge of the stop band γ_1 has been chosen, the value of y_1 can be computed from Eq. (37), and ϵ may then be computed from Eq. (36); thus the response of a five-element fan type of birefringent filter is completely specified.

The next step is to put Eq. (35) in the form of a Fourier cosine series, which is then identified as M_{11} of Eq. (28):

$$P_5\left(\frac{\cos \gamma}{y_1}, \epsilon\right) = A_5 \cos 5\gamma + A_3 \cos 3\gamma + A_1 \cos \gamma \equiv M_{11}(\gamma) \quad , \tag{38}$$

where the A_k ($k = 1, 3,$ and 5) coefficients are functions of ϵ and γ_1. Now, making use of the defining equation for Chebyshev polynomials,

$$T_k(\cos\gamma) = \cos(k\gamma) \quad , \quad k \text{ an integer} \quad , \tag{39}$$

we make the following substitutions in Eq. (38):

$$\cos(3\gamma) = 4\cos^3\gamma - 3\cos\gamma \tag{40}$$

and

$$\cos(5\gamma) = 16\cos^5\gamma - 20\cos^3\gamma + 5\cos\gamma \quad . \tag{41}$$

After gathering like terms and equating coefficients of the same power of $\cos\gamma$ in Eqs. (35) and (38), the following are obtained:

$$\begin{aligned} 16A_5 &= 16\frac{\epsilon}{y_1^5} \quad , \\ -20A_5 + 4A_3 &= -20\frac{\epsilon}{y_1^3} \quad , \\ 5A_5 - 3A_3 + A_1 &= 5\frac{\epsilon}{y_1} \quad . \end{aligned} \tag{42}$$

Equations (42) are solved in an iterative manner to yield the coefficients of Eq. (38):

$$\begin{aligned} A_5 &= \epsilon y_1^{-5} \\ A_3 &= 5\epsilon\left(y_1^{-5} - y_1^{-3}\right) \\ A_1 &= 5\epsilon\left(2y_1^{-5} - 3y_1^{-3} + y_1^{-1}\right) \quad . \end{aligned} \tag{43}$$

Finally, an exponential Fourier series is constructed from Eq. (38):

$$M_{11}(\gamma) = \left(\frac{A_5}{2}\right) e^{j5\gamma} + \left(\frac{A_3}{2}\right) e^{j3\gamma} + \left(\frac{A_1}{2}\right) e^{j\gamma} + \left(\frac{A_1}{2}\right) e^{-j\gamma} + \left(\frac{A_3}{2}\right) e^{-j3\gamma} + \left(\frac{A_5}{2}\right) e^{-j5\gamma} \quad . \tag{44}$$

Equation (44) is in a form suitable for use with the Harris synthesis procedure, which is given in the following paragraph in outline only. Equations (35), (38), and (44), which are all identical functions of γ are approximately sketched in Fig. 18.

3. Harris's Synthesis Procedure

The procedure makes use of the coefficients of the two exponential series that describe the desired filter output and the orthogonal (undesired) output. Since only the Fourier series of the desired output can be found in the direct manner described above, the first step in synthesis is to find the orthogonal output. (We assume, at this point, that the coefficients of $M_{11}(\gamma)$ have been computed for a particular value of γ_1.) The orthogonal output is obtained by invoking the principle of the conservation of energy. Accordingly, the following equation is true at all frequencies:

$$|M_{11}|^2 + |M_{21}|^2 = 1 \quad . \tag{45}$$

This equation states that the total output power normalized to the input power is unity at all frequencies in a lossless, nonreflective, birefringent filter. Equation (45) is then solved for $|M_{21}|^2$:

$$|M_{21}|^2 = 1 - |M_{11}|^2 \quad . \tag{46}$$

Now, M_{21} is in the form of an exponential series for the same reasons that M_{11} is.[7,14] The problem is how to find that series, given $|M_{21}|^2$. This is explained by Harris,[7] using a procedure described by Pegis that includes complex root-finding methods. During this process, one-half of a set of 2N roots are chosen for use in the ensuing operations, and

the remaining roots are discarded. The correct roots to choose are those with absolute magnitude less than or equal to one.

After the exponential series M_{21} has been found, a matrix multiplication method is used to sequentially find the plate difference angles ρ_i. This series of steps starts with finding the output polarizer difference angle $\rho_P = \beta_p - \beta_N$, and then works backwards from the last plate difference angle, ρ_N, to the first, ρ_1, thereby obtaining the ρ_i of every pair of elements in the filter. Then, by changing the signs of alternate ρ_i of the fan-type filter, we obtain the design of a folded-type filter, and finally, the plate angles β_i. As explained earlier, this also requires a change of the output plane of polarization from the direct to the orthogonal wave, but this change is automatically accomplished by the sign reversal of all the alternate ρ_i, including ρ_p.

4. An Equal-Ripple Design (N = 5)

The response shape of an optimum design is shown in Fig. 19, for a folded-type filter, with N = 5. The abscissa is the variable γ. Since the response is symmetrical with respect to γ = 90 degrees, only the lower stop band and half of the first pass band are shown. The edge of the stop band is $\gamma_1' = 43.4$ degrees, and the ripple level is $\epsilon = 0.02$. (Figure 19 gives the relative power output, hence ϵ^2 is shown there as the peak power of the ripples in the stop band.) Although the curve of Fig. 19 was originally found by an approximate method employed before all the details of the exact synthesis procedure had been worked out and programmed on a computer, it is close enough to the exact curve as to be indistinguishable from it to the scale drawn. Likewise, the plate angles shown in Fig. 19, which also were obtained by an approximate method, are accurate to the significant figure shown. The exact plate angles obtained from the synthesis by computer are

$$\beta_1 = \beta_5 = 4.90240 \text{ degrees}$$

$$\beta_2 = \beta_4 = -10.1365 \text{ degrees}$$

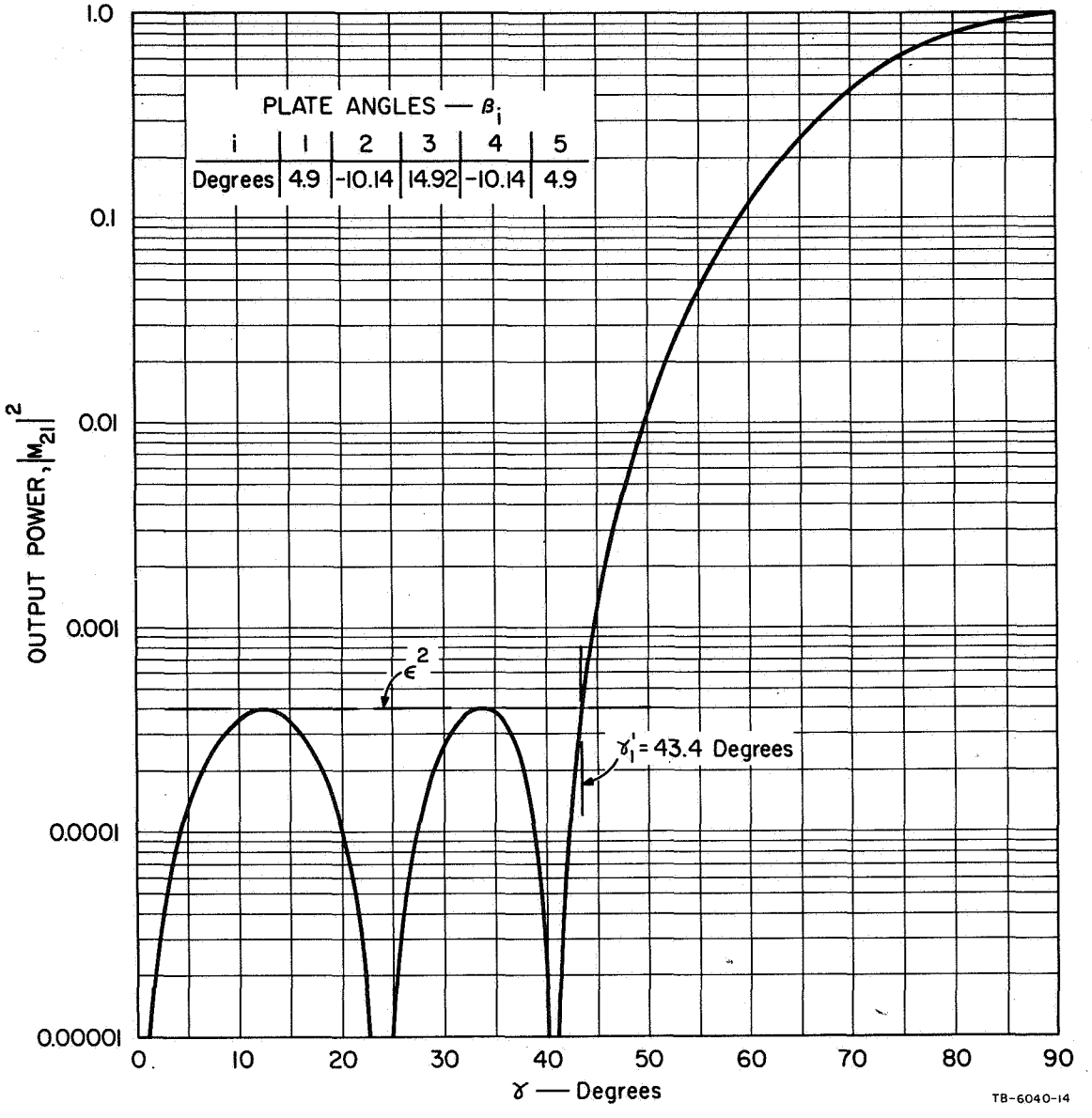

FIG. 19 COMPUTED RELATIVE POWER OUTPUT OF A FOLDED TYPE OF EQUAL-RIPPLE FIVE-ELEMENT FILTER

$$\beta_3 = 14.9221 \text{ degrees}$$

$$\beta_p = 90.0 \text{ degrees} \quad .$$

The input for the computer synthesis was $\gamma_1 = 46.6$ degrees for the fan-type filter, corresponding with $\gamma_1' = 90 - 46.6 = 43.4$ degrees, the edge of the stop band of the folded-type filter response of Fig. 19.

5. Synthesis of Maximally Flat Stop-Band Response Filters

The maximally-flat condition is met when all possible derivatives with respect to the variable y in $P_N(y)$ (including the 0^{th}-order derivative, i.e., the function itself) are set equal to zero at y = 0. This is done by letting all but the N^{th} coefficients of the terms in the polynomial equal zero. Since there are N such terms, N of the (N + 1) allowed degrees of freedom are used. The last remaining choice is to make the output unity at the design frequency, which is done by making the N^{th} coefficient equal 1, yielding

$$P_N(y) = y^N \quad . \tag{47}$$

Then with the usual substitution,

$$\cos \gamma = y \quad , \tag{48}$$

we obtain the matrix element M_{11} of the fan filter

$$M_{11} = \cos^N \gamma \quad . \tag{49}$$

When Eq. (49) is expressed as an exponential Fourier series, the coefficients of the terms of the series are found to be the binomial coefficients of order N. Likewise, the coefficients of $|M_{11}|^2$ in the expression $1 - |M_{11}|^2$ of the orthogonal (power) output are the binomial coefficients of order 2N. From this point on, the synthesis proceeds by the Harris method, as for the equal-ripple case in part 3 of this section (B-3), except that no auxiliary parameters such as ε and γ_1 of

the equal-ripple case enter into the synthesis procedure. However, in order to choose a suitable value of N for a given application, it is necessary to know the relationship between N and a suitable defined band-edge parameter. Using the 3-dB point as the band-edge parameter in γ, we have [from Eq. (49)] for the fan-type filter,

$$\cos \gamma_1 = (1/2)^{1/2N} , \tag{50}$$

from which the band-edge birefringence parameters γ_1 and $\gamma_1' = 90 - \gamma_1$ (for the fan- and folded-type filters, respectively) may be computed.

6. Formulas for Equal-Ripple Filters with Any Value of N

In order to compute the plate angles for any value of N and various values of γ_1, the following iterative formulas were developed. These formulas give the Chebyshev coefficients, the coefficients of the two Fourier exponential series M_{11} and $|M_{21}|^2$, and the coefficients of the polynomial (A8) of the Pegis procedure, as described in Harris.[7]

a. Chebyshev Coefficients

The coefficient of y^k of the N^{th}-order Chebyshev polynomial of the first kind $T_N(y)$ is given the notation t_{Nk} for N both even and odd. An iterative formula for the t_{Nk} is then

$$t_{Nk} = 2t_{N-1,\,k-1} - t_{N-2,k} , \text{ for } k = 1 \text{ to } N , \tag{51}$$

with the following initial conditions:

$$\begin{aligned} t_{N0} &= (-1)^{N/2}, \text{ for N even,} \\ t_{N0} &= 0, \text{ for N odd,} \\ t_{11} &= 1, \\ t_{N-2,\,k} &= 0, \text{ for } k > (N-2). \end{aligned}$$

b. Coefficients of the Fourier Exponential Series M_{11}

First compute ϵ from the Chebyshev coefficients*

$$\epsilon^{-1} = \sum_{k=1}^{N} t_{Nk} y_1^{-k} \quad , \quad \text{for k odd} \quad . \tag{52}$$

We then have for the coefficients of the cosine series,

$$A_{N-k} = \frac{1}{t_{N-k,\,N-k}} \left(\epsilon \frac{t_{N,\,N-k}}{y_1^{N-k}} - \sum_{j=2}^{\frac{k+2}{2}} A_{N-2(j-2)} t_{N-2(j-2),\,N-k} \right) \quad . \tag{53}$$

The A_{N-k} values are to be computed for even values of k, over the range k = 0 to N - 1. Note that if k = 0 in this equation, the summation term is understood to be zero. The coefficients of the exponential series $M_{11} = C_o + C_2 e^{-j2\gamma} + C_4 e^{-j4\gamma} + \ldots + C_{n-2} e^{-j(N-2)\gamma} + C_N e^{-jN\gamma}$ are then obtained from the A_{N-k} values as follows:

$$C_j = C_{n-j} = \frac{1}{2} A_{N-2j} \quad , \quad j = 0 \text{ to } \frac{(N-1)}{2} \quad . \tag{54}$$

These are analogous to the coefficients of $C(\omega)$ in Harris's Eqs. (2) and (20)[7] and are given in the same order. Here, unlike its function in the previous cosine series, the subscript j does not directly indicate the power of the exponential variable.

c. Coefficients of the Exponential Series $|M_{21}|^2$

$$D_0 = 1 - \sum_{k=0}^{N} C_k^2 \tag{55}$$

and

$$D_k = - \sum_{j=0}^{N-k} C_j C_{j+k} \quad , \quad \text{for k = 1 to N} \quad .$$

* An alternate procedure, replacing Eq. (52), would be to choose ϵ and compute y_1 from Eq. (39) as was done in the footnote on page 42.

Here, again, the D_k coefficients are analogous to those of $D(\omega)$ in Harris's Eqs. (8) and (21), and they are given in the same order.[7]

d. Coefficients B_k of Eq. (A8) in Harris's Method

First, construct the following set of numbers:

$$R_{jk} = R_{j-1,\,k-1} + R_{j,\,k-2} \quad , \quad j = 0 \text{ to } N,\ k = j \text{ to } N \quad , \tag{56}$$

excluding those R_{jk} in which $(j + k)$ is an odd number, with the initial conditions

$$R_{jj} = 1 \text{ for all } j$$
$$R_{0k} = 2 \text{ for } k \neq 0.$$

The coefficients of the Pegis polynomial [coefficients of y^k in Eq. (A8) in Harris et al[7]] are then computed for k = 0 to n:

$$B_k = \sum_{j=0}^{N-k} (-1)^{j/2} R_{k,\,k+j} D_{k+j} \quad , \tag{57}$$

with the summation over j to be made only for even values of $j \leq (n - k)$.

The remainder of the synthesis procedure is as given in Harris et al[7]; it requires complex root-finding procedures, the reconstruction of the polynomial M_{21} from half of the root factors of $|M_{21}|^2$, and matrix multiplications for determining plate angles. As mentioned in part 3 of this section (B-3), the proper roots of $|M_{21}|^2$ to use in the synthesis procedure are those with absolute magnitude less than or equal to one.

The iterative formulas in this section were obtained by arraying the various end-product terms in two-dimensional arrays and then looking for rules that allowed the construction of the terms in a given row from the terms in the previous row (or rows). In the case of the coefficients B_k, this necessitated the prior solution of the problem for each value of N up to N = 9.

e. Discussion

Of further interest, from the network theory viewpoint, are the computer-determined distributions of the one real zero and the $(N - 1)/2$ pair of conjugate zeros of the Pegis Eqs. (A8) and (A10) in Harris.[7] These equations describe the orthogonal wave response $|M_{21}|^2$ and M_{21}, respectively, of the fan-type filter. Here, the variables appear to be $Y = 2 \cos 2\gamma$ and $X = e^{j2\gamma}$. When the zeros of Eq. (A8) for $|M_{21}(Y)|^2$ are plotted in the complex Y-plane, they are found to lie on an ellipse, the major axis of which lies on the real axis. The roots are equi-spaced on the ellipse in the sense that they are projections (toward the real axis) of N equi-spaced points on the circumscribing circle, with conjugate roots in both the right and left half-planes, and the one real root at the vertex of the ellipse $Y = 2$. The semi-major diameter of the ellipse is $\underline{a} > 2$, hence the center of the ellipse does not lie on the origin but is slightly displaced to the left thereof. The locus of the half-cycle in γ, $0 < \gamma < \pi/2$ (see the lower left sketch of Fig. 3, which shows a full cycle of the orthogonal response of the fan-type filter) is thus transformed to $0 < 2\gamma < \pi$, and in the variable Y, it is $-2 < Y < 2$ on the real axis. As noted above, the point $Y = 2$ is a vertex of the ellipse; the point $Y = -2$ appears to be the opposite focus of the ellipse. This distribution of zeros is to be compared with the zeros of $|M_{21}|^2$ in the variable y/y_1, which can be derived for the general case by substituting (a generalized version of) Eq. (33) into Eq. (46):

$$|M_{21}|^2 = 1 - \epsilon^2 T_N^2\left(\frac{y}{y_1}\right) \quad . \tag{58}$$

Here, the zeros can be shown to lie on an ellipse centered on the origin, with 2N zeros that are equi-spaced on the ellipse in the same sense as stated above: the locus $0 < \gamma < \pi/2$ is transformed to $0 < y/y_1 < 1$ on the real axis of y/y_1. The exact location of the zeros, derived by a method illustrated by Weinberg,[16] are

$$\left(\frac{y}{y_1}\right)_k = \frac{y_k}{y_1} = \cos\left(\frac{k\pi}{N}\right)\cosh\phi -$$

$$j \sin\left(\frac{k\pi}{N}\right)\sinh\phi,\ k = 0, 1, 2, .. 2N - 1 \quad ,$$

where

$$\phi = \frac{1}{N}\cosh^{-1}\frac{1}{\epsilon} = \cosh^{-1}\frac{1}{y_1} \quad . \tag{59}$$

It is natural to ask what is the relationship between these two zero distributions, and how can we derive one from the other? The answer to these questions would make it possible to find the zeros of M_{21} by formula, without the need for general (polynomial) root-finding procedures, as was done here for the tabulated optimum-response filter designs.

The computer-determined zeros of $M_{21}(X)$ are found to lie on a pear-shaped curve with its vertex at $X = 1(\gamma = 0)$, with one real zero at $X = 1$, and $(N - 1)/2$ pairs of conjugate zeros (absolute magnitude less than one) arrayed around the origin, on the rounded portion of the curve, which is almost circular in shape. The locus of the half-cycle in γ, $0 < \gamma < \pi/2$, is here the unit circle starting at $X = 1(\gamma = 0)$ and ending on $X = -1$. As explained in Harris,[7] the zero locations are obtained from those of $|M_{21}(Y)|^2$ by the solution of a quadratic equation.

V DESIGN TABLES FOR OPTIMUM RESPONSE FILTERS

The design tables in this section give the plate angles β_i of the folded-type filter for all odd values of N from N = 5 to 19, and for N = 25 (see Figs. 3 and 19). In each case, five separate designs are given for various values of the stop-band ripple parameter ϵ. The tables give the value of ϵ in terms of attenuation L_s, defined by

$$L_s = 20 \log_{10} \epsilon^{-1} \text{ dB} \quad . \tag{60}$$

The output wave is orthogonal to the input wave for these designs. Heading each column are values of L_s from 10 to 40 dB. These are, however, only nominal values. The exact attenuation values, from which the tables were computed, are within 0.1 dB of the nominal values for most of the cases listed, the greatest deviation from the nominal value being 0.22 dB, and these exact values are given directly below the last given value of β_i for each case. Since the folded-type filter is symmetrical about a central plane, only the first half of the β_i values, including i = (N + 1)/2, is given in the tables. The angle γ_1' [from which L_s (exact) was computed] is also given for each design. Remembering that γ_0 = 90 degrees is the center of the pass band for the folded-type filter and that the response has arithmetic symmetry about γ_0, the relative width of the first pass band at the ϵ level may readily be computed as follows:

$$w = \frac{90 - \gamma_1'}{90} \quad . \tag{61}$$

The value of $\underline{w}$ thus obtained relates to the first pass band; higher-order pass bands (all odd) will have relative bandwidths inversely proportional to their order.

The approximate values of attenuation used for synthesizing the filter designs were found by interpolation in published tables of the

squared Chebyshev function[17] listed against values of N and y_1^{-1}. A direct approach would have been to solve the equation in the footnote (p. 42) for exact values of y_1 for given values of ϵ. Such a course would have added little to the utility of the final results. Several of the designs, including N = 25, were analyzed by the matrix multiplication technique of Eq. (26), and the responses at the ripple peaks were found to be within a few hundredths of a dB of the exact value of attenuation. The β_i values (i = 1 to N) were computed in sequential order from β_N to β_1 and were found to be symmetrical to better than 0.001 degree for the N = 25 designs, and to better than 0.0001 degree for the designs with lower values of N, with increasing symmetry as N decreases. Since the tables give β values that are rounded off to the fourth decimal place (in degrees), all listed values except for N = 25 retain the full accuracy of the computations; for N = 25 there is some (but not complete) loss of accuracy in the last decimal place. In any case, the precision of the tables generally exceeds the state of the art of setting devices to precise angles.

A previously unsuspected feature of equal-ripple designs that is brought out by the tables is the fact that many of the designs (those with the smaller L_s values) have β values that do not alternate in sign. They do, however, alternate in position about some average (non-zero) value of β and are therefore of the folded-type design. The corresponding fan-type filters have monotonically increasing β values, and both types, of course, are symmetrical, or anti-symmetrical, about a central plane.

The value of γ' for a 3-dB loss in the pass band may be computed from the following formula:

$$\gamma'_{3dB} = \sin^{-1}\left[\sin \gamma'_1 \cosh \frac{0.115}{N}(L_s + 3)\right] \quad . \qquad (62)$$

The primed values of γ denote the folded-type filter, and the values of γ'_1 and L_s (attenuation) are given in the design tables.

Equation (62) is accurate for ripple levels of 10 dB or greater and may therefore be used with all the design tables in this report.

DESIGN TABLES FOR EQUAL-RIPPLE STOP BAND (FOLDED-TYPE) BIREFRINGENT FILTERS

Table I: N = 5

ATTENUATION (NOMINAL)	10	15	20	30	40
GAMMA/1PRIME (DEGREES)	69.62	63.44	57.55	47.20	38.26
BETA[I]	15.0843	11.0060	8.3863	5.5708	4.1994
(DEGREES)	1.4638	-3.7661	-6.8380	-9.6124	-10.5991
I=1,2,3,...	17.7590	15.4277	14.5513	14.6327	15.4030
ATTENUATION (EXACT)	9.99	14.95	20.03	29.95	39.97

Table II: N = 7

ATTENUATION (NOMINAL)	10	15	20	30	40
GAMMA/1PRIME (DEGREES)	75.27	70.63	66.22	57.94	50.18
BETA[I]	13.1514	8.9231	6.3180	3.5400	2.2297
(DEGREES)	4.1609	-0.4030	-2.8306	-4.7216	-5.0604
I=1,2,3,...	15.0415	12.0154	10.5452	9.6391	9.6754
	3.0640	-2.3182	-5.6122	-9.1972	-11.0692
ATTENUATION (EXACT)	10.01	15.01	20.00	29.94	40.12

Table III: N = 9

ATTENUATION (NOMINAL)	10	15	20	30	40
GAMMA/1PRIME (DEGREES)	78.52	74.81	71.29	64.49	58.01
	12.2189	7.9079	5.3422	2.6692	1.4881
BETA[I]	5.5991	1.2546	-0.9591	-2.5860	-2.7683
(DEGREES)	13.4851	9.9470	8.0665	6.4334	5.8674
I=1,2,3,...	4.6174	-0.4392	-3.3744	-6.3675	-7.7108
	14.0249	10.9210	9.5154	8.8880	9.3104
ATTENUATION (EXACT)	9.97	15.02	20.00	29.99	40.08

Table IV: N = 11

ATTENUATION (NOMINAL)	10	15	20	30	40
GAMMA/1PRIME (DEGREES)	80.60	77.52	74.59	68.88	63.44
	11.6500	7.3122	4.7790	2.2103	1.1369
	6.4361	2.1904	0.0516	-1.5044	-1.6861
BETA[I]	12.5368	8.7176	6.6216	4.6525	3.8504
(DEGREES)	5.6706	0.8958	-1.7551	-4.2131	-5.0760
I=1,2,3,...	13.1038	9.7262	8.0984	7.0802	7.1592
	5.3679	0.3396	-2.5950	-5.6780	-7.1829
ATTENUATION (EXACT)	9.95	15.03	20.02	30.02	39.95

Table V: N = 13

ATTENUATION (NOMINAL)	10	15	20	30	40
GAMMA/1PRIME (DEGREES)	82.01	79.42	76.93	72.06	67.30
	11.1941	6.9274	4.4348	1.9503	0.9319
	6.9025	2.7831	0.6798	-0.8779	-1.1009
BETA[I]	11.8489	7.9430	5.7442	3.6283	2.7283
(DEGREES)	6.3065	1.8026	-0.6588	-2.8045	-3.4221
I=1,2,3,...	12.3454	8.8010	6.9728	5.5685	5.2864
	5.9486	1.1604	-1.6126	-4.4211	-5.7017
	12.5332	9.1461	7.4974	6.4989	6.6558
ATTENUATION (EXACT)	10.00	15.02	19.99	29.93	39.94

Table VI: N = 15

ATTENUATION (NOMINAL)	10	15	20	30	40
GAMMA/1PRIME (DEGREES)	83.05	80.85	78.66	74.35	70.18
	10.8630	6.6976	4.2036	1.7541	0.7997
	7.2211	3.2224	1.0996	-0.4938	-0.7516
BETA[I]	11.3645	7.4587	5.1765	2.9691	2.0575
(DEGREES)	6.7509	2.4703	0.0859	-1.9076	-2.3914
I=1,2,3,...	11.7806	8.1554	6.1594	4.4707	3.9620
	6.4123	1.8815	-0.7770	-3.3279	-4.3253
	12.0202	8.5843	6.8065	5.5984	5.5822
	6.2880	1.6549	-1.1251	-3.9569	-5.2607
ATTENUATION (EXACT)	10.04	14.95	19.95	30.02	39.99

Table VII: N = 17

ATTENUATION (NOMINAL)	10	15	20	30	40
GAMMA/1PRIME (DEGREES)	83.90	81.89	79.91	76.16	72.42
	10.7368	6.4550	3.9559	1.6278	0.7100
	7.5764	3.4739	1.3341	-0.2301	-0.5267
	11.1272	7.0490	4.7096	2.5424	1.6315
BETA[I]	7.2039	2.8786	0.5400	-1.2964	-1.7256
(DEGREES)	11.4683	7.6187	5.5037	3.7038	3.0571
I=1,2,3,...	6.9083	2.3657	-0.2028	-2.4644	-3.2662
	11.7047	8.0419	6.1364	4.7599	4.5339
	6.7432	2.0629	-0.6664	-3.2743	-4.4500
	11.7896	8.2000	6.3821	5.2018	5.1982
ATTENUATION (EXACT)	9.97	15.02	20.13	30.00	40.07

Table VIII: N = 19

ATTENUATION (NOMINAL)	10	15	20	30	40
GAMMA/1PRIME (DEGREES)	84.46	82.69	81.06	77.62	74.25
	10.3247	6.2072	3.9209	1.5434	0.6519
	7.5363	3.6035	1.6268	-0.0373	-0.3723
	10.6469	6.6864	4.5129	2.2537	1.3526
BETA[I]	7.2246	3.1188	1.0021	-0.8627	-1.2765
(DEGREES)	10.9393	7.1600	5.1467	3.1632	2.4377
I=1,2,3,...	6.9609	2.6760	0.3892	-1.8074	-2.4866
	11.1647	7.5506	5.7035	4.0756	3.6782
	6.7826	2.3590	-0.0737	-2.6051	-3.6255
	11.2883	7.7746	6.0363	4.6718	4.5615
	6.7193	2.2430	-0.2481	-2.9250	-4.1108
ATTENUATION (EXACT)	10.19	15.17	19.86	29.92	39.92

Table IX: N = 25

ATTENUATION (NOMINAL)	10	15	20	30	40
GAMMA/1PRIME (DEGREES)	85.79	84.46	83.10	80.50	77.93
	10.0028	5.9436	3.5236	1.3333	0.5309
	8.0157	4.0553	1.9087	0.2708	-0.1179
	10.1765	6.2152	3.8607	1.7175	0.8882
	7.8453	3.7784	1.5518	-0.1700	-0.5664
	10.3410	6.4925	4.2309	2.2080	1.4263
BETA[I]	7.6895	3.5063	1.1767	-0.6991	-1.1853
(DEGREES)	10.4854	6.7529	4.6006	2.7599	2.1086
I=1,2,3,...	7.5596	3.2645	0.8241	-1.2528	-1.9038
	10.5974	6.9691	4.9231	3.2898	2.8257
	7.4689	3.0810	0.5452	-1.7297	-2.5725
	10.6646	7.1132	5.1455	3.6833	3.3933
	7.4257	2.9816	0.3903	-2.0112	-2.9870
	10.6852	7.1640	5.2250	3.8303	3.6125
ATTENUATION (EXACT)	10.15	15.09	20.22	30.15	40.06

VI CONCLUSION

The mechanics of adapting the theory of optical birefringent filters to millimeter wavelengths appears to be fairly straightforward. The concept of impedance-matched elements, which leads to design and analysis methods within the present state of the art, can be implemented with artificial anisotropic dielectric media; however, the resulting designs may not be the most compact that can be made with a given bulk dielectric material. Hence, the methods described herein are only a beginning in this area.

Extrapolation of the results of research on the microwave scale model (reported herein) to millimeter wavelengths should not be difficult. The necessarily smaller size and greater fragility of the resulting structure would then demand different methods of manufacture from the standard machining techniques used for the scale model. This does not appear to be an insurmountable problem for half-wave plates with a center frequency as high as 90 GHz, where the thickness of a plate lamination would be about 0.025 inch. Nevertheless, plate designs embodying anisotropic dielectrics that are easier to construct than the air-dielectric sandwich type of material used here might be preferred for use at such short wavelengths.

The optimum-response birefringent-filter design tables, their derivation and the numerical tables, represent an important advance in the state of the art; the analytical techniques and the numerical results should prove useful at optical as well as millimeter wavelengths. The methods used in deriving the optimum-response filter designs can also be used for other useful network components, such as differential phase-shifters and directional couplers. Topics relating to artificial anisotropic dielectrics that are worthy of investigation include (1) improved methods of construction aimed at making them light, compact, and inexpensive; and (2) study of the effects of reflections from interfaces between plates and between a plate and free space, and means of dealing with such effects.

VII RECOMMENDATIONS FOR FUTURE WORK

Problems encountered and suggestions for solving them are given below:

1. Edge tapers on the laminations of the birefringent plate described herein increased its length by more than fifty percent compared with a uniform plate. It would, therefore, be desirable to seek a means to eliminate tapered edges, perhaps by close spacing of uniform plates, without, of course, causing any significant degradation in filter performance.

2. The positions of the upper pass bands and stop bands depend on higher-order effects in plates with large spacings (that is, large compared with a wavelength) between laminations. Further investigation of these effects would provide information on the upper frequency limits of specific birefringent structures.

3. A birefringent filter with a small number of plates, that operates in its lowest passband, will not have a very narrow passband. For this reason it would be desirable to combine a birefringent filter with an easier-to-construct multilayer interference filter having a narrow passband.

4. An interference filter of the type mentioned in (3) above could be tuned by inclination and thus could be used to suppress spurious passbands of the birefringent filter.

REFERENCES

1. Leo Young, B. M. Schiffman and C. A. Hacking, Proposal for Research, SRI No. ELU 65-27, "Novel Millimeter and Submillimeter Wave Filters," Stanford Research Institute, Menlo Park, California (10 February 1965).

2. B. Lyot, "Optical Apparatus with Wide Field Using Interference of Polarized Light," Comptes Rendus, Vol. 197, pp 1593-1595 (1933).

3. I. Solc, "A New Type of Birefringent Filter," Czech. J. of Phys., Vol. 4, No. 1, pp 53-66 (1954), AD 140-058.

4. I. Solc, "Further Investigation of the Birefringent Filter," Czech. J. of Phys., Vol. 5, No. 1, pp 80-86 (1955), AD 140-058.

5. I. Solc, "Chain Birefringent Filters," Czech. J. of Phys., Vol. 9, pp 237-249 (1959).

6. I. Solc, "Birefringent Chain Filters," J. Opt. Soc. Am., Vol. 55, pp 621-625 (June 1965).

7. S. E. Harris, E. O. Ammann, and I. C. Chang, "Optical Network Synthesis Using Birefringent Crystals: I. Synthesis of Lossless Networks of Equal-Length Crystals," J. Opt. Soc. Am., Vol. 54, pp 1267-1279 (October 1964).

8. S. E. Harris and C. M. McIntyre, "Achromatic Waveplates for the Visible Spectrum," Paper presented at the Conference on Electron Device Research, McGill University, Montreal, Canada, June 21-23, 1967.

9. W. H. Steel, R. N. Smartt, and R. G. Giovanelli, "A 1/8 Angstrom Birefringent Filter for Solar Research," Aust. J. Phys., Vol. 14, No. 2, pp 201-211 (June 1961).

10. R. E. Collin, "A Simple Artificial Anisotropic Dielectric Medium," IRE Trans. on Microwave Theory and Tech., Vol. MTT-6, pp 206-209 (April 1958).

11. J. W. Evans, "Solc Birefringent Filter," J. Opt. Soc. Am., Vol. 48, pp 142-145 (March 1958).

12. R. C. Jones, "New Calculus for the Treatment of Optical Systems. I. Description and Discussion of the Calculus," J. Opt. Soc. Am., Vol. 31, p 488 (1941).

13. C. L. Dolph, "A Current Distribution for Broadside Arrays which Optimizes the Relationship Between Beamwidth and Side-Lobe Level," Proc. IRE, Vol. 34, pp 335-348 (June 1946).

14. L. Mertz, "A Fourier Description of Optical Interference Devices, Part II," J. Opt. Soc. Am., Vol. 50, advertisement facing p xii (June 1960).

15. E. O. Ammann, "Optical Network Synthesis Using Birefringent Crystals. III. Some General Properties of Lossless Birefringent Networks," J. Opt. Soc. Am., Vol. 56, pp 943-951 (July 1966).

16. L. Weinberg, Network Analysis and Synthesis (McGraw-Hill Book Co., Inc., New York, N.Y., 1962) pp 507-532.

17. Leo Young, "Multilayer Interference Filters with Narrow Stop Bands," Applied Optics, Vol. 6, pp 297-315 (February 1967).

ACKNOWLEDGMENTS

The assistance of Messrs. John Herndon and Walter Wiebenson, Jr. of the Mathematical Sciences Department, and of Mr. Philip Reznek of the Electromagnetic Techniques Laboratory, in programming the filter analysis and synthesis is gratefully acknowledged.

Mr. Mauro Di Domenico, Sr., performed the laboratory measurements on the birefringent plate and filter.

NASA-Langley, 1967 —— 9 CR-979

"The aeronautical and space activities of the United States shall be conducted so as to contribute . . . to the expansion of human knowledge of phenomena in the atmosphere and space. The Administration shall provide for the widest practicable and appropriate dissemination of information concerning its activities and the results thereof."

—NATIONAL AERONAUTICS AND SPACE ACT OF 1958

NASA SCIENTIFIC AND TECHNICAL PUBLICATIONS

TECHNICAL REPORTS: Scientific and technical information considered important, complete, and a lasting contribution to existing knowledge.

TECHNICAL NOTES: Information less broad in scope but nevertheless of importance as a contribution to existing knowledge.

TECHNICAL MEMORANDUMS: Information receiving limited distribution because of preliminary data, security classification, or other reasons.

CONTRACTOR REPORTS: Scientific and technical information generated under a NASA contract or grant and considered an important contribution to existing knowledge.

TECHNICAL TRANSLATIONS: Information published in a foreign language considered to merit NASA distribution in English.

SPECIAL PUBLICATIONS: Information derived from or of value to NASA activities. Publications include conference proceedings, monographs, data compilations, handbooks, sourcebooks, and special bibliographies.

TECHNOLOGY UTILIZATION PUBLICATIONS: Information on technology used by NASA that may be of particular interest in commercial and other non-aerospace applications. Publications include Tech Briefs, Technology Utilization Reports and Notes, and Technology Surveys.

Details on the availability of these publications may be obtained from:

SCIENTIFIC AND TECHNICAL INFORMATION DIVISION

NATIONAL AERONAUTICS AND SPACE ADMINISTRATION

Washington, D.C. 20546